JOURNAL OF AIRCRAFT
Vol. 54, No. 4, July–August 2017

Integrated Assessment of Aircraft and Novel Subsystem Architectures in Early Design

Imon Chakraborty* and Dimitri N. Mavris†
Georgia Institute of Technology, Atlanta, Georgia 30332

DOI: 10.2514/1.C033976

The aerospace industry's progressive transition toward More Electric subsystem architectures presents some unique challenges for the early design stages: in part, due to the unavailability of historical data and the presence of a large number of subsystem architecture possibilities. Such novel subsystem architectures, which may have a pronounced effect on aircraft performance, must therefore be considered earlier in the design process than conventional architectures have traditionally been. This paper demonstrates the integration of aircraft and engine sizing with explicit sizing and analysis of the subsystems, using models and methods that are suitable for the early design phases. The resulting Integrated Subsystem Sizing and Architecture Assessment Capability is used to investigate a subsystem architecture design space for three aircraft sizes. The assessment reveals a characteristic clustering of subsystem architectures driven by the design characteristics of a few subsystems. It also reveals subsystem design solution trends existing in the best-performing subsystem architectures for each aircraft size. A sensitivity analysis is also performed to determine the impact of uncertainties in the secondary power extraction penalties on the performance of an electrified subsystem architecture.

I. Introduction

THE aircraft equipment systems [1], such as the environmental control system (ECS), the ice protection systems (IPSs), and the actuation systems for flight controls, landing gear, thrust reversers, brakes, and nose-wheel steering, all provide functionalities to the aircraft that are necessary for safe flight. The power used for the operation of these subsystems, which may be pneumatic, hydraulic, or electric [2,3], is called non-propulsive or secondary power. In conventional designs (Fig. 1, left), pneumatic power (compressed air extracted from the engines) is used to operate the ECS and IPS. Mechanical shaft-power drawn off the engine is used to drive hydraulic pumps and electric generators to generate hydraulic and electric power, respectively. The hydraulics power the aircraft actuation functions, whereas electricity is used for avionics, lighting, and other cabin loads. Such conventional solutions, though reliable, have nevertheless reached technology saturation. This fact and the rapidly improving state-of-the-art of electric drives and power electronics [2,4] have resulted in the More Electric Initiative, which is a renewed interest in electrically powered subsystems. The potential benefits, which include possible aircraft-level weight reduction, increased efficiency, and reconfigurability [3], have prompted several notable research programs, technology demonstrations, and numerous feasibility studies [5–9]. In commercial aviation, the industry's progressive approach has thus far resulted in More Electric Aircraft (MEA) [10,11], in which some (but not all) subsystems have been electrified. An All Electric Aircraft (AEA), in which all subsystems are electrically powered (Fig 1, right), has not yet materialized in service. Even so, the large number of MEA possible through the electrification of different combinations of subsystems yields a challenging combinatorial problem that did not exist previously.

Presented as Paper 2016-0215 at the 54th AIAA Aerospace Sciences Meeting, San Diego, CA, 4–8 January 2016; received 14 April 2016; revision received 21 August 2016; accepted for publication 11 September 2016; published online 20 December 2016.

*Research Engineer II, Aerospace Systems Design Laboratory, School of Aerospace Engineering. Member AIAA.

†S.P. Langley Distinguished Regents Professor and Director of Aerospace Systems Design Laboratory, School of Aerospace Engineering. Fellow AIAA.

Historically, aircraft conceptual design has focused primarily on the sizing of the vehicle and its propulsion system in order to meet given mission performance and point performance requirements. This phase is dominated by considerations of aerodynamics, propulsion, and weight estimation, each of which is potentially affected by the subsystems. For instance, subsystems that require admission of ram air through incorporation of ram air inlets directly affect the aerodynamics. Subsystem secondary power extraction of any kind increases the specific fuel consumption of the propulsion system. Finally, there is the obvious impact of subsystems on aircraft weight. Due to the large number of aircraft designs with conventional subsystem solutions, designers have access to a large historical database, heuristic rules that aid in accounting for subsystem effects during early design, and statistical regression equations for subsystem weights [12–14]. The fact that such resources are not available for the case of MEA/AEA clearly poses a design challenge. The combinatorial problem described previously and the sub-optimal solutions at the vehicle-level that would likely result from designing More Electric subsystems in isolation [1] pose additional challenges.

The approach to addressing these challenges that is presented in this work shares some commonalities with prior work by other researchers [15,16] in that 1) subsystem sizing is driven by flowdown of top-level aircraft and mission requirements, and 2) the impact of mass, power off-takes, and drag penalties of the sized subsystems is linked back to the aircraft performance analysis. However, it differs from prior works in one or more of the following:

1) A parsimonious modeling approach, which uses parameters that are either available or estimable in early design, is undertaken.

2) Large-scale interpolation from results of prior studies is avoided, as well as the use of restricted subsystem data or models not available in the public domain.

3) The combinatorial problem for MEA/AEA architectures is addressed explicitly by assessing a diverse subset of the architecture design space.

4) The variation in subsystem architecture impact with aircraft size is assessed by considering multiple aircraft baselines spanning a wide range of gross weights.

5) The connectivity among subsystem architecture elements is determined using heuristic rules to ensure redundancy equivalent to that provided by current design practices.

6) It is possible to systematically decompose the net impact of each subsystem architecture into contributions from constituent subsystems' masses, power off-takes, and drag increments. Interdependencies between aircraft-level and subsystem-level parameters are established within an integrated sizing and analysis

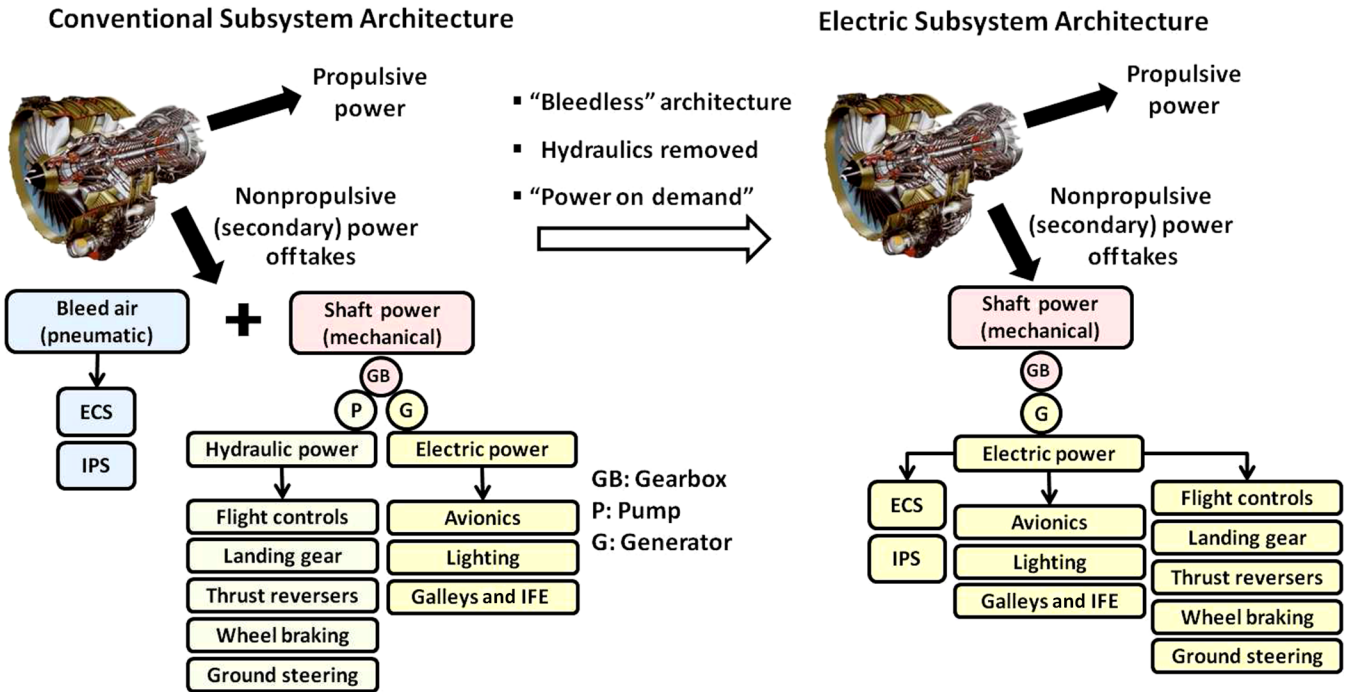

Fig. 1 Secondary power usage by major subsystems within conventional and electric subsystem architectures.

environment, whereby the aircraft and its subsystems are simultaneously resized until convergence. The resultant of this approach, the Integrated Subsystem Sizing and Architecture Assessment Capability (ISSAAC), permits the conceptual designer of MEA/AEA to assess the performance of subsystem architectures for aircraft that have identical point and mission performance capabilities, as well as the impact that sources of uncertainty have on said performance.

The remainder of this paper is organized as follows: Sec. II describes the main modules of ISSAAC. Section III introduces the aircraft, the subsystems, and the subset of the architectural design space that are subsequently analyzed. Section IV provides a brief description of the modeling approach for each subsystem considered. Section V investigates the identified architecture design space for the selected aircraft baselines and the sensitivity of an electrified architecture to uncertainties in the penalties associated with secondary power extraction. Finally, Sec. VI concludes the paper and identifies some avenues for future research.

II. Overview of Integrated Subsystem Sizing and Architecture Assessment Capability

The main ISSAAC modules are depicted in Fig. 2. Though the current implementation of ISSAAC is with a certain set of tools, the underlying approach itself is not tool specific and only requires that the chosen tools collectively have the following functionalities: 1) aircraft sizing and mission performance analysis capability, 2) propulsion cycle analysis capability, 3) subsystem sizing and analysis capability, and 4) analysis integration capability (for sequencing execution of functions 1–3, passing relevant information between modules, and checking for analysis convergence). Further, the same tool may be used to satisfy more than one of the aforementioned functions. ISSAAC currently uses MATLAB to perform functions 3 and 4; the Flight Optimization System (FLOPS), which is a tool developed by the NASA Langley Research Center [17] for function 1; and the Numerical Propulsion System Simulation [18] to generate the engine performance characteristics for function 2. Each module is described in brief as follows, and the interested reader is referred to a separate work [19] for a more thorough account:

1) *Definition of design requirements*: These include the mission performance requirements (e.g., payload-range envelope), the point performance requirements, and the aircraft notional concept (for which this work considers aft-tailed tube-and-wing turbofan commercial transport designs). Three aircraft sizes, each described in greater detail in Sec. III.A, are considered.

2) *Traditional aircraft & engine sizing*: Within this module, the goal is to define the aircraft in terms of a geometric scale (represented by the wing planform area S_w), a propulsive scale (represented by the required sea-level static thrust T_{SL}), and key weights such as the takeoff gross weight W_{TO} and the empty weight W_E. The mission performance analysis yields the fuel requirement W_F and the vehicle weight fractions β corresponding to the stated point performance requirements. The constraint analysis yields the thrust-to-weight ratio (T/W or, to be precise, $T_{\mathrm{SL}}/W_{\mathrm{TO}}$) and wing loading ($W/S$ or, to be precise, W_{TO}/S_w) that allow the point performance requirements to be met. The sizing process is driven by 1) aerodynamic characteristics such as lift vs angle of attack (C_L vs α) and the drag polar (C_D vs C_L); 2) propulsive characteristics such as the thrust lapse $T = f(h, M)$ and specific fuel consumption variations $sfc = f(h, M, P_{\mathrm{np}})$ with altitude, Mach number, and non-propulsive power off-take P_{np}; and 3) estimation of the vehicle's empty weight or empty weight fraction W_E/W_{TO}. The weight buildup relationships within FLOPS (and most other similar tools) are based on regressions of historical data, and therefore apply to conventional subsystem architectures. Thus, for the first iteration, an aircraft with conventional subsystem architecture serves as the starting point for the remaining modules.

3) *Candidate subsystem architecture descriptor*: This provides a qualitative description of the subsystem architecture to be evaluated in terms of the design solutions for each of the subsystems (e.g., pneumatic versus electric ECS, hydraulic versus electric actuation functions, etc.). For the automated investigation of a large number of subsystem architectures, the descriptors are obtained from a matrix of alternatives (MOAs), as shown in Fig. 2. The development of the MOA for this work is discussed further in Sec. III.C.

4) *Subsystem architecture sizing and evaluation*: This module performs the sizing of the major power consuming elements, power distribution elements, and power sources within the subsystem architecture (a generalized representation of which is shown in Fig. 3a). The subsystems considered and the modeling approach for each are described in Sec. IV. The modeling approach allows the impact of epistemic uncertainty and technological state-of-the-art (SOTA) on predicted subsystem performance to be assessed through the incorporation of variation factors that are commonly referred to as

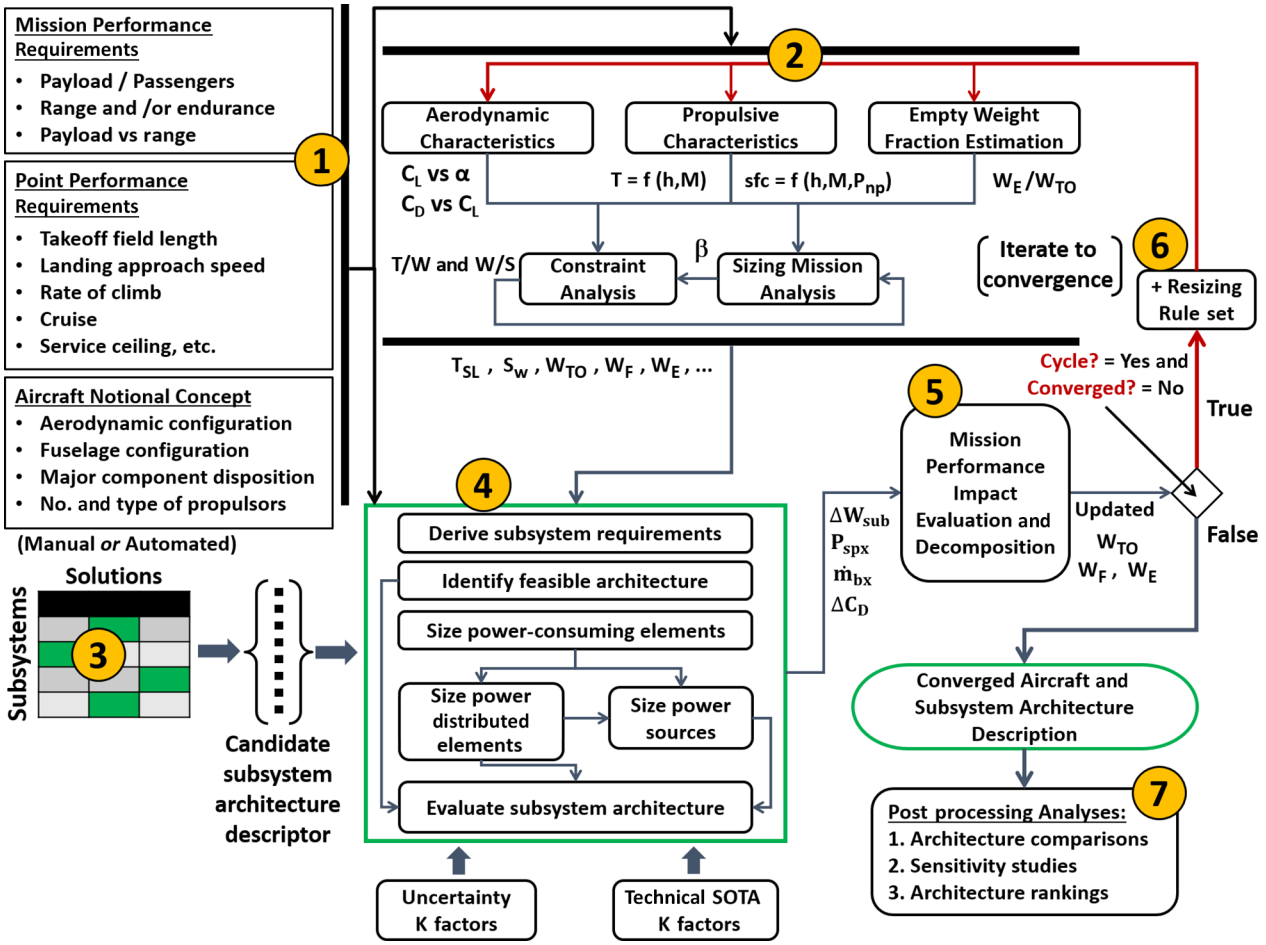

Fig. 2 Main modules of Integrated Subsystem Sizing and Architecture Assessment Capability.

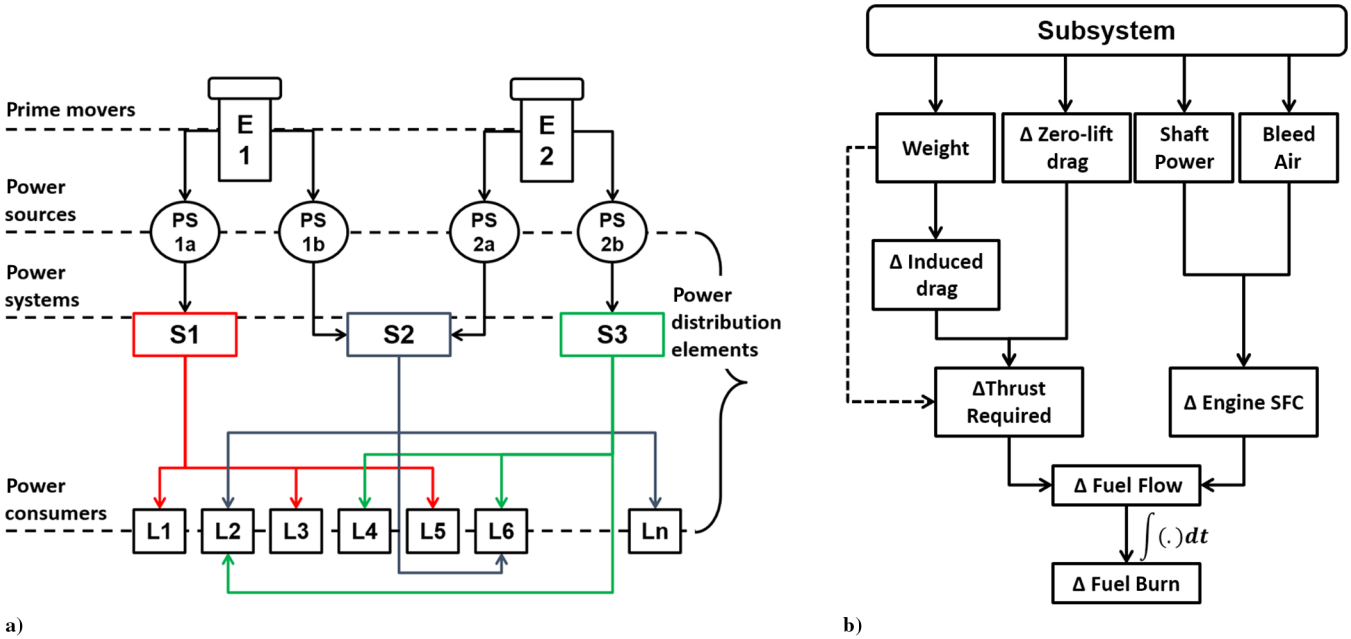

a) b)

Fig. 3 Representations of a) elements and connectivity within an aircraft subsystem architecture and b) impact of subsystems on fuel consumption (mission-level metric).

K factors [20]. The outputs of this module are the difference in weight ΔW_{sub} of the considered architecture relative to a conventional one, and the time histories of the architecture's shaft-power requirement $P_{\text{spx}}(t)$, bleed air requirement $\dot{m}_{\text{bx}}(t)$, and direct drag increment $\Delta C_D(t)$. The latter three time-varying quantities are computed for each subsystem and for the whole architecture.

5) *Mission performance impact evaluation and decomposition*: The purpose of this module is to re-evaluate the impact of the subsystem architecture on the mission performance using the information generated by the previous modules. The subsystem architecture affects a mission-level metric such as fuel consumption through weight, secondary power requirements, and drag increments, as shown in Fig. 3b. First, the impact of the architecture weight change ΔW_{sub} is computed by propagating the computed subsystem weights to the FLOPS mission performance analysis through the appropriate weight override factors [17]. Next, the effects of the time-varying shaft-power requirement $P_{\text{spx}}(t)$, bleed air requirement $\dot{m}_{\text{bx}}(t)$, and direct drag increments $\Delta C_D(t)$ are computed from fundamental considerations of changes in lift, drag, thrust, and fuel flow caused by these at each point within an invariant mission profile that terminates with a certain (constant) landing fuel reserve. Subject to these assumptions, the additional fuel $\Delta W_f^{(\text{TO})}$ required at takeoff on account of $P_{\text{spx}}(t)$, $\dot{m}_{\text{bx}}(t)$, and $\Delta C_D(t)$ is computed by solving the following equation system backward in time (from landing where $k = n$ to takeoff where $k = 1$), with the intent of computing the takeoff fuel increment $\Delta W_f^{(\text{TO})} = \Delta W_f^{(1)}$:

$$\Delta C_L^{(k)} = \frac{\Delta W^{(k+1)}}{((1/2)\rho V^2)^{(k)} S_w} = \frac{\Delta W_f^{(k+1)}}{((1/2)\rho V^2)^{(k)} S_w} \tag{1a}$$

$$\Delta C_{D_i}^{(k)} = C_{D_i}\left(C_{L,0}^{(k)} + \Delta C_L^{(k)}\right) - C_{D_i}\left(C_{L,0}^{(k)}\right) \tag{1b}$$

$$\Delta D_{\text{ddl}}^{(k)} = \left(\frac{1}{2}\rho V^2\right)^{(k)} S_w \Delta C_{D_i}^{(k)} \tag{1c}$$

$$\Delta D_{\text{dil}}^{(k)} = \left(\frac{1}{2}\rho V^2\right)^{(k)} S_w \Delta C_{D_0}^{(k)} \tag{1d}$$

$$\Delta D^{(k)} = \Delta D_{\text{ddl}}^{(k)} + \Delta D_{\text{dil}}^{(k)} \tag{1e}$$

$$\Delta T^{(k)} = \Delta D^{(k)} + \Delta W^{(k+1)}\left(\frac{\dot{h}}{V} + \frac{\dot{V}}{g}\right)^{(k)} \tag{1f}$$

$$T^{(k)} = T_0^{(k)} + \Delta T^{(k)} \tag{1g}$$

$$\Delta \dot{w}_f^{(k)} = \dot{w}_f\left(T^{(k)}, h^{(k)}, M^{(k)}, P_{\text{spx}}^{(k)}, \dot{m}_{\text{bx}}^{(k)}\right) - \dot{w}_f\left(T_0^{(k)}, h^{(k)}, M^{(k)}, 0, 0\right) \tag{1h}$$

$$\Delta W^{(k)} = \Delta W_f^{(k)} = \Delta W^{(k+1)} + \Delta \dot{w}_f^{(k)} \Delta t^{(k)} \tag{1i}$$

$k = k - 1$, and repeat sequence. Start point:

$$k = n - 1, \qquad \Delta W^{(n)} = 0$$

The computed parameters in the preceding equation system are as follows: C_L is lift coefficient, C_{D_i} is the induced drag coefficient, C_{D_0} is the zero-lift drag coefficient, D_{ddl} is the drag dependent on lift, D_{dil} is the drag independent of lift, D is the total drag, T is the thrust, $\dot{w}_f$ is the fuel flow, W is the vehicle gross weight, W_f is the fuel weight, h is the altitude, V is the velocity, M is the Mach number, and $((1/2)\rho V^2)$ is the dynamic pressure. The symbol Δ denotes the increment of a parameter relative to its value $()_0$ for an identical reference mission that does not consider the effect of secondary power extraction and drag increments.

6) *Re-sizing of aircraft & subsystems*: This module governs an iterative re-sizing of the aircraft and its subsystems in accordance with certain re-sizing rules. In this work, subsystem architectures are compared while ensuring that the aircraft containing them have identical mission performance capabilities (such as payload and range) and point performance capabilities. With regard to the latter, a feasible design that satisfies necessary point performance requirements may be represented by its wing loading (W_{TO}/S_w) and thrust-to-weight ratio ($T_{\text{SL}}/W_{\text{TO}}$). Currently, the assumption is made that a sufficient margin exists between the aforementioned feasible design point and proximate constraint curves so that shifts in the latter on account of subsystem architecture changes are not sufficient to render the design point infeasible. Subject to this assumption, the requirement that a constant thrust-to-weight ratio and wing loading be maintained is imposed. This resizing rule results in the following relationships for updating the wing area S_w and engine thrust rating T_{SL}:

$$\Delta S_w = \frac{\Delta W_{\text{TO}}}{(W_{\text{TO}}/S_w)} - \frac{W_{\text{TO}}}{(W_{\text{TO}}/S_w)^2}\Delta\left(\frac{W_{\text{TO}}}{S_w}\right)$$

$$\Delta T_{\text{SL}} = \left(\frac{T_{\text{SL}}}{W_{\text{TO}}}\right)\Delta W_{\text{TO}} + \Delta\left(\frac{T_{\text{SL}}}{W_{\text{TO}}}\right)W_{\text{TO}}$$

Additionally, a second resizing rule is imposed by requiring that constant stabilizer volume ratios be maintained. This is intended to represent invariant stability and control requirements, and it is subject to the underlying assumption that center-of-gravity shifts on account of subsystem architecture changes do not significantly alter tail moment arms. The resizing process terminates when the magnitudes of residuals for the gross weight ΔW_{TO}, wing loading $\Delta(W_{\text{TO}}/S_w)$, and thrust-to-weight ratio $\Delta(T_{\text{SL}}/W_{\text{TO}})$ fall below specified thresholds.

7) *Post-processing analyses*: This is a customizable module depending on the type of analysis being performed, and may include different means for data tabulation or visualization. The following postprocessing analyses are presented within the scope of this paper:

a) Comparative assessments of the weight and fuel impacts of a large number of subsystem architectures for three aircraft sizes (Sec. V.A).

b) Ranking of the best-performing architectures for three aircraft sizes in order to detect trends in subsystem designs that appear in the ranking (Sec. V.B).

c) Sensitivity study analyzing the impact of variations in secondary power extraction penalties on the performance of an electrified subsystem architecture (Sec. V.C).

III. Downselection of Aircraft and Subsystem Architecture Space

A. Selection of Vehicle Baselines

To assess the effect of aircraft size on the performance of subsystem architectures, three aircraft sizes are selected: 1) Small Single-Aisle Aircraft (SSA), 2) Large Twin-Aisle Aircraft (LTA), and 3) Very Large Aircraft (VLA). Representative aircraft models are created based on public-domain geometry information for in-service commercial aircraft of these three types and high-bypass ratio turbofan engines for the corresponding thrust classes (Table 1). A limited calibration exercise was performed to obtain acceptable agreement between predicted and published weight and mission performances (fuel consumption) for each of the three aircraft. This yields the reference SSA, LTA, and VLA baselines for the subsystem architecture sizing and analysis trades described in the subsequent sections of the paper.

B. Selection of Subsystems to be Considered

The aircraft subsystems considered in the scope of this paper (shown in Fig. 4) are divided into two categories: 1) power generation and distribution subsystems (PGDSs) and 2) power-consuming subsystems. Four PGDSs are considered for 1) electric power (EPGDS), 2) hydraulic power (HPGDS), 3) pneumatic power

Table 1 Data summary for SSA, LTA, and VLA baselines[a]

Aircraft data	Aircraft identification		
	SSA	LTA	VLA
Passenger capacity	170	396	852
Design range, n mile	3,000	7,800	8,200
Cruise Mach number	0.785	0.84	0.85
Maximum ramp weight, lb	175,130	746,610	1,270,000
Sea-level static thrust, lbf	$2 \times 26{,}244$	$2 \times 114{,}220$	$4 \times 69{,}872$
Wing planform area, ft^2	1,347	4,695	9,111
Wingspan, ft	114.8	201.8	266.4
Wing taper ratio	0.24	0.15	0.21
Wing 1/4-chord sweep, deg	25	31.6	30
HT planform area, ft^2	305	1,089	2,212
Horizontal tail (HT) aspect ratio	5.47	4.50	4.49
HT taper ratio	0.37	0.30	0.39
HT 1/4-chord sweep, deg	30	35	35
Vertical tail (VT) planform area, ft^2	231	562	1,316
VT aspect ratio	1.80	1.60	1.74
VT taper ratio	0.30	0.29	0.39
VT 1/4-chord sweep, deg	30	35	37
Fuselage length, ft	123.3	239.8	230.9
Fuselage maximum width, ft	12.9	20.3	23.4
Fuselage maximum height, ft	12.9	20.3	27.9

[a]In each case, tabulated data correspond to an aircraft with conventional subsystem architecture (hydraulic actuation, pneumatic ECS and IPS, and no Electric Taxiing System).

(PPGDS), and 4) mechanical power (MPGDS). For architectures where no hydraulic or pneumatic power is used, the HPGDS or PPGDS is removed entirely.

The actuation subsystems, comprising the Flight Controls Actuation System (FCAS), the Landing Gear Actuation System (LGAS), the Nose-Wheel Steering System (NWSS), the Wheel Braking System (WBS), and the Thrust Reverser Actuation System (TRAS) may use either hydraulic or electric power (indicated by the arrows in Fig. 4). Similarly, the ECS, Wing Ice Protection System (WIPS), and Cowl Ice Protection System (CIPS) may use either pneumatic or electric power. Finally, some architectures may contain an optional Electric Taxiing System (ETS), in which Auxiliary Power Unit (APU)-powered electric motors drive the main gear wheels and allow taxiing with the main engines turned off [9].

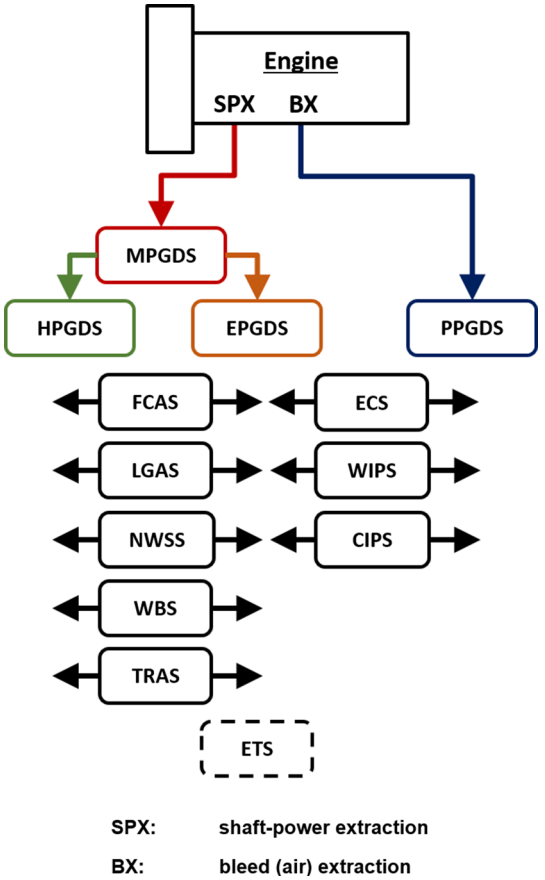

Fig. 4 Summary of power-consuming subsystems and power generation and distribution subsystems considered within the scope of this work.

C. Generation of Subsystem Architecture Description

The presence of multiple subsystems and multiple design solutions for each subsystem results in the generation of a very large combinatorial space of subsystem architectures. In fact, in the work of Chakraborty and Mavris [21], it was shown that in excess of $13 \cdot 10^6$ architecture combinations would arise by considering only a partial enumeration of possible design solutions for the power-consuming subsystems shown in Fig. 4. The required computational time may, in such cases, make an exhaustive evaluation of the architecture space infeasible. Therefore, this work uses a subspace of the architectural design space for which the exhaustive evaluation is tractable yet which retains diverse subsystem architecture possibilities (enumerated in Table 2). This architectural subspace was arrived at by 1) not considering minor architectural perturbations about a conventional baseline; 2) eliminating certain subsystem technologies known to be infeasible; and 3) considering a progressive, packaged electrification of the actuation functions (for details, the reader is referred to [19]). The successive actuation packages $P-0, \ldots, P-7$ (described in Table 3) involve electrification of progressively more flight-critical actuation functions. The IPS solutions differ in 1) secondary power type (pneumatic vs electric), 2) magnitude of supplied heat flux (in evaporative systems, supplied heat is sufficient to completely evaporate impinging water, unlike in running-wet systems), 3) mode of operation (anti-ice systems work continuously to prevent any ice formation, whereas de-ice systems activate periodically to dispatch ice buildup). The architectures considered are described by the candidate subsystem architecture descriptor scheme explained in Fig. 5. Thus, the conventional baseline architectures for the three aircraft are denoted by SSA-00000, LTA-00000, and VLA-00000.

IV. Overview of Subsystem Modeling Approach

As the subsystems affect fuel consumption through multiple avenues (Fig. 3b), one of the end goals of the subsystem modeling approach is to be able to characterize subsystems in terms of 1) weight w_{sub}; as well as the time histories of 2) shaft-power requirement $P_{\text{spx}}(t)$ (if any), 3) bleed air requirement $\dot{m}_b(t)$ (if any), and 4) direct drag increment $\Delta C_D(t)$ (if any). Due to the number of subsystems considered, it is not feasible to describe in detail the modeling approach for each subsystem. Therefore, only a brief overview is provided for each, and the interested reader is referred to separate works for an in-depth description [19,22].

A. Actuation Functions

The first step for evaluating the actuation subsystems (FCAS, LGAS, NWSS, WBS, and TRAS) is to determine the actuation load or power requirements, which is described briefly in the following sections for each actuation function. The actuator mass is determined based on the actuation load or actuation power that it is sized to provide using the following relationship:

$$M_{\text{act}} = \frac{\mathcal{X}_0}{(\mathcal{X}_0/M)} + \frac{P_m^{\max}}{\eta_m}\left\{\frac{1}{(P/M)_{\text{em}}}\left(\frac{1}{\kappa_{\text{em}}}-1\right) + \frac{1}{\eta_{\text{em}}\eta_{\text{pe}}(P/M)_{\text{pe}}}\left(\frac{1}{\kappa_{\text{pe}}}-1\right)\right\} \tag{2}$$

In Eq. (2), $\mathcal{X}_0$ may represent the stall load for a linear actuator, the maximum output moment $\mathcal{M}_0$ of a rotary hinge-line actuator, or the maximum shaft-power output of a power drive unit.

Table 2 Reduced combinatorial space of subsystem architectures assessed in this paper[a,b,c]

Subsystem	Options[a]	No.
Actuation functions	Packages *P*-0, . . . , *P*-7	8
Wing ice protection	P-Ev-AI, P-RW-AI, E-RW-AI, E-RW-DI	4
Cowl ice protection	P-Ev-AI, P-RW-AI, E-EV-AI, E-RW-AI	4
Environmental control system	Pneumatic, electric	2
Electric taxiing system	Present, absent	2

[a]Actuation packages are explained in Table 3.
[b]For IPS designs, P denotes pneumatic, E denotes electrothermal, Ev denotes evaporative, RW denotes running-wet, AI denotes anti-icing, and DI denotes de-icing.
[c]Total combinations are equal to 512.

Table 3 Packaged electrification of actuation functions[a,b]

	Actuation package no.							
Actuation function	P-0	P-1	P-2	P-3	P-4	P-5	P-6	P-7
TRAS	— —	√	√	√	√	√	√	√
WBS	— —	√	√	√	√	√	√	√
LGAS	— —	— —	√	√	√	√	√	√
NWSS	— —	— —	√	√	√	√	√	√
FCAS-HLD	— —	— —	— —	√	√	√	√	√
FCAS-Sp.	— —	— —	— —	EHA	EMA	EMA	EMA	EMA
FCAS-THSA	— —	— —	— —	— —	√	√	√	√
FCAS-Prim.	— —	— —	— —	— —	— —	H/EHA	EHA	EMA

[a]Electrification is indicated either by a checkmark (√) or by the name of the type of actuator(s) employed.
[b]EHA denotes electrohydrostatic actuator, EMA denotes electromechanical actuator, H/EHA denotes hydraulic actuator and EHA in parallel, HLD denotes high-lift devices, THSA denotes trimmable horizontal stabilizer actuator, Sp. denotes spoilers, and Prim. denotes primary flight control surfaces.

The corresponding figure of merit $(\mathcal{X}_0/M)$ is then, respectively, a force-to-mass ratio, a moment-to-mass ratio, or a power-to-mass ratio. For electric actuators, the power-to-mass ratios of the electric motor and the power electronics with current technological state-of-the-art are represented by $(P/M)_{\text{em}}$ and $(P/M)_{\text{pe}}$, respectively. Their overall efficiencies are represented by η_{em} and η_{pe}, respectively. The overall efficiencies of electric actuator components downstream of the electric motor output shaft are collectively represented by η_m. Improvements in the SOTA are represented by $\kappa_{\text{em}} > 1$ and $\kappa_{\text{pe}} > 1$, which result in a reduction in the actuator mass predicted by Eq. (2).

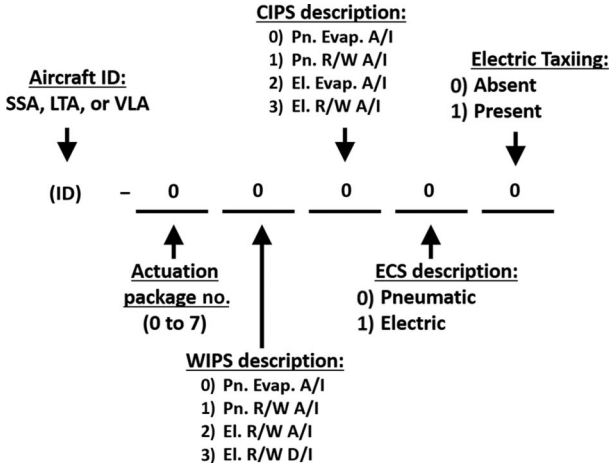

Fig. 5 Definition of candidate subsystem architecture descriptor (ID, identification; Pn, pneumatic; Evap, evaporative; El, electrothermal).

1. Flight Controls Actuation System

For the FCAS, flight control surfaces are defined relative to the lifting surfaces based on early design sizing guidelines [12,23]. Thus, as the aircraft resizes, the control surface dimensions change with changes in the geometry of the parent lifting surfaces. For hinged control surfaces such as ailerons, elevators, rudder, and spoilers, the actuation loads are computed using hinge moment coefficients [24] and relevant constraining flight conditions [25]. The actuation power requirements are computed using assumed control surface duty cycles [26]. For the high-lift devices and the trimmable horizontal stabilizer actuator (THSA), the actuation power requirements are computed based on data from existing aircraft and actuators [19].

2. Wheel Braking System

Brake actuation requirements are determined from constraining static and dynamic braking cases. Static cases correspond to parking on an inclined surface and holding the aircraft stationary during a full-throttle engine runup. Dynamic cases include rejected takeoff (accelerate-stop case) at maximum takeoff weight (MTOW) and landing deceleration at maximum landing weight [27], which are described in more detail in Title 14 of the Code of Federal Regulations (CFRs), Section 25.735 [28]. Applying force and moment balances, the deceleration requirements are translated to corresponding braking torques based on the tire geometry [29] and further to brake actuator output forces based on the brake dimensions [30].

3. Nose-Wheel Steering System

The NWSS actuation requirements are computed by considering 1) a load condition specified in Title 14 of the CFRs, Section 25.499 [28] (aircraft at maximum ramp weight, a dynamic load factor $\kappa = 1.33$, and a critical horizontal load at the tire-to-ground contact point of 0.8 times the normal reaction); and 2) the moment required to turn the nose-wheel while the aircraft is stationary (with tire scrubbing) [31]. Steering moments corresponding to these loading conditions are computed using the NWSS geometry, which is set based on preliminary guidelines for the class of aircraft considered [12].

4. Landing Gear Actuation System

The LGAS actuation requirements are computed using a simplified model of the retraction/extension kinematics [22] and based on the mass properties of the gear legs (which are related to the aircraft MTOW [32]). The underlying assumption is that the gravitational load dominates over the aerodynamic, frictional, and inertial loads [33]. The mechanism kinematics permit the computation of the actuator's peak output force and stroke. The actuator maximum rate is computed based on the stroke and the retraction/extension time requirement. The LGAS is evaluated following the evaluation of the WBS, NWSS, and ETS (if installed), whose masses and locations affect the landing gear actuation load.

5. Thrust Reverser Actuation System

Only very limited information on thrust reverser power requirements is found in the open literature. A flow rate for the CFM56 engine is available from work by Scholz [34], and the electrical power rating (in kilonewtons) for the Airbus A380 ETRAS is available [35]. Based on only these two data points, the power requirement per engine for the TRAS is estimated as a linear function of the rated sea-level thrust of a single engine:

$$P_{\text{tras}}[\text{kV} \cdot \text{A or kW}] = 0.047\, T_{\text{SL}}[\text{kN}] + 10.782, \text{ (per engine)} \quad (3)$$

in which the power is assumed to be in kilovolt amperes for electric TRAS and in equivalent kilowatts for hydraulic TRAS. In the latter case, the equivalent kilowatt figure is converted into a corresponding flow requirement using the hydraulic power equation.

B. Wing Ice Protection System and Cowl Ice Protection System

The electric or pneumatic power requirements for ice protection at a given flight condition depend on 1) the surface area A_{prot} to be protected and 2) the required total heat flux $\dot{q}_{\text{tot}}$ for that flight condition. For the WIPS, a study conducted by Airbus noted that the mean aerodynamic chord (MAC) c_{mac} had a significant influence on the spanwise extent of the WIPS protected area [16]. The spanwise extent $\Delta\eta_{\text{wips}}$, which was normalized by wing semispan, was noted as decreasing with c_{mac}. Based on this observation, geometric information for several commercial aircraft was used to develop the following regression expressing $\Delta\eta_{\text{wips}}$ as a function of c_{mac} (expressed in meters) [19]:

$$\Delta\eta_{\text{wips}} = \kappa_0 + \kappa_1 c_{\text{mac}}[m] + \kappa_2 (c_{\text{mac}}[m])^2,$$
$$\kappa_0 = 0.3933, \quad \kappa_1 = 0.0372, \quad \kappa_2 = -0.005 \tag{4}$$

The CIPS protected area was parameterized based on the nacelle diameter and length.

The total heat flux $\dot{q}_{\text{tot}}$ required to maintain a desired protected surface temperature T_{skin} against an ambient temperature T_∞ is computed as the resultant of four heat transfer processes: convection, sensible heating, evaporation, and kinetic heating:

$$\dot{q}_{\text{tot}} = \dot{q}_{\text{conv}} + \dot{q}_{\text{sens}} + \dot{q}_{\text{evap}} + \dot{q}_{\text{kin}} \tag{5}$$

For a given flight and atmospheric condition, each of these four components is estimated using well-established relationships [36,37]. To find the WIPS and CIPS sizing points, the total heat flux $\dot{q}_{\text{tot}}$ is computed over a three-dimensional search grid $\mathcal{G}$: $\{h, V_\infty, T_\infty\}$, where $h - V_\infty$ combinations are selected within the aircraft flight envelope. The $h - T_\infty$ combinations are set based on the Continuous Maximum Icing (CMI) and Intermittent Maximum Icing (IMI) envelopes defined in Title 14 of the CFRs, Section 25, Appendix C [28]; or the European Aviation Safety Agency's CS-25, Appendix C [38]. Following established practice, the CMI conditions, in which the aircraft is considered to be exposed to relatively lower liquid water content (LWC) for an extended period of time, are used for sizing the WIPS [15,39]. IMI conditions, where the aircraft is considered to be exposed to relatively larger LWC for a relatively shorter period of time, are used to size the CIPS [15,39]. The sizing point is identified as the flight condition yielding the maximum required total heat flux $\dot{q}_{\text{tot}}^{\max}$.

For the pneumatic IPS, the heat requirement is translated to a corresponding bleed air requirement using an overall system heat transfer efficiency $\eta_{p-\text{wips}}$ (assumed to be ≈65% [15,16]) as

$$\dot{m}_{\text{bleed}} = \frac{\dot{q}_{\text{tot}} A_{\text{prot}}}{\eta_{p-\text{wips}} C_{p,a} (T_{\text{supply}} - T_s)} \tag{6}$$

where T_{supply} is the temperature of the bleed air supplied to the pneumatic IPS. For the electrothermal IPS, the required electrical power is computed following the work of Krammer and Scholz [37] as

$$P_{\text{elec}} = \frac{A_{\text{prot}}}{\eta_{\text{heat}}} \cdot \{\dot{q}_{\text{ps}} \kappa_{\text{ps}} + \dot{q}_{\text{cyc}} (1 - \kappa_{\text{ps}}) \kappa_{\text{cyc}}\} \tag{7}$$

where $\dot{q}_{\text{ps}} = \dot{q}_{\text{tot}}$ is the continuous heat flux supplied to spanwise and chordwise parting strips that cover $\kappa_{\text{ps}} \in [0, 1]$ fraction of the total protected area, $\dot{q}_{\text{cyc}}$ is the cyclic heat flux provided to cyclic heaters which have an activity ratio of $\kappa_{\text{cyc}} \in [0, 1]$, and the heating arrangement is assumed to have an efficiency of η_{heat}.

For mass estimation, the anti-icing system mass estimate provided by FLOPS is first used along with the total protected lengths for the WIPS and CIPS to compute a mass per unit length, which is then used to compute the individual pneumatic WIPS and CIPS masses. For electrothermal designs, data provided by Al-Khalil et al. [36], consisting of the densities and thicknesses of the materials forming the heated area of an electrothermal design, is used to compute the effective mass per unit area. Also, the mass of power control equipment is computed based on the maximum system power requirement and the assumed power-to-mass ratio of power electronics. For electrothermal de-icing designs, a drag penalty is assessed using an empirical correlation given by Gray [40].

C. Environmental Control System

The ECS analysis assumes 1) a constant desired cabin temperature of $T_{\text{cab}} = 24°\text{C}$, uniform throughout the cabin and constant throughout the flight [41], 2) a cabin pressure P_{cab} set as a function of altitude based on a pressurization schedule [42], and 3) a nominal volume flow rate per occupant of $\dot{\mathcal{V}}_{\text{perocc.}} = 20\ \text{ft}^3/\text{min}$ [43]. The nominal mass flow rate $\dot{m}_{\text{cab}}$ supplied to the cabin is computed from T_{cab}, P_{cab}, $\dot{\mathcal{V}}_{\text{perocc.}}$, and cabin occupancy using the ideal gas relationship. Using a lumped thermal analysis and a steady-state heat balance, the required temperature T_{in} of air supplied to the cabin is computed as

$$T_{\text{in}} = T_{\text{cab}} + \frac{\dot{Q}_{\text{loss}} - \dot{Q}_{\text{int}}}{\dot{m}_{\text{cab}} C_p} \tag{8}$$

The heat loss $\dot{Q}_{\text{loss}}$ through the cabin wall is computed as $\dot{Q}_{\text{loss}} = (T_{\text{cab}} - T_{\text{aw}})/R_{\text{tot}}$, where T_{aw} is the adiabatic wall temperature and R_{tot} the total thermal resistance across the fuselage wall. The internal heat load $\dot{Q}_{\text{int}}$ consists of the metabolic heat load per passenger [44] (assumed to be $\dot{Q}_{\text{meta}}/N_{\text{pax}} = 75$ W), the power consumption of in-flight entertainment systems [45], (assumed to be $\dot{Q}_{\text{ife}}/N_{\text{pax}} = 50$ W), and galley loads [45] (assumed to be $\dot{Q}_{\text{galley}}/N_{\text{pax}} = 320$ W).

Since modern ECS designs employ recirculation [43], ϵ_{recirc} is used to denote the fraction of the air extracted from the cabin that is subsequently recirculated. The application of mass and energy balances allows the calculation of the mass flow rate $\dot{m}_{\text{pack}}$ and the pack discharge temperature T_{pack} for each of N_{pack} packs as

$$\dot{m}_{\text{pack}} = \frac{(1 - \epsilon_{\text{recirc}})}{N_{\text{pack}}} \dot{m}_{\text{cab}}, \quad T_{\text{pack}} = \frac{T_{\text{in}} - \epsilon_{\text{recirc}} T_{\text{cab}}}{1 - \epsilon_{\text{recirc}}} \tag{9}$$

For the conventional (pneumatic) ECS, this mass flow rate is extracted as bleed air from the engines, and therefore imposes a fuel consumption penalty. For an electric ECS, this mass flow rate is admitted through ram air inlets and then passes through a diffuser. The compression of the air from post-diffusion pressure to pack entry pressure using electric Cabin Air Compressors (CACs) imposes a shaft-power extraction penalty.

The conditioning of the pack mass flow rate $\dot{m}_{\text{pack}}$ to the pack exit temperature T_{pack} is achieved through the modulation of the mass flow rate $\dot{m}_{\text{ram}}$ of ram air that serves as the heat sink. This ram air mass flow rate throughout the mission is computed by solving a thermodynamic model of the ECS pack (shown in Fig. A1 of the Appendix), in which the layout of components is determined based on inspection of Airbus and Boeing documents available in the public domain [46–50]. Although electric ECS solutions may feature customized ECS pack designs [5], conventional bootstrap units may also be considered within an electric ECS scheme [6]. Therefore, for simplicity, the same pack architecture is assumed for both the conventional and electric ECS solutions. The drag increment due to the admission of this ram air is conservatively estimated by assuming complete momentum loss, yielding $\Delta D_{\text{ram}} = N_{\text{pack}} \dot{m}_{\text{ram}} V_\infty$. For electric ECS designs, where the pack air $\dot{m}_{\text{pack}}$ is also admitted as ram air, the ram drag increment is assessed as $\Delta D_{\text{ram}} = N_{\text{pack}} (\dot{m}_{\text{ram}} + \dot{m}_{\text{pack}}) V_\infty$.

Since the same pack design is assumed for both the pneumatic and electric ECS solutions, there is no variation in the mass of the ECS packs between the two architectures. An estimate of the air conditioning system mass is obtained directly from FLOPS, which includes the mass of the ECS packs of the conventional architecture. For the electric ECS, the additional mass of the CACs, motors, and the power electronics is computed as

$$M_{\text{cac}} = \frac{P_{\text{cac}}^{\max}}{(P/M)_{\text{cac}}} = \frac{P_{\text{elec}}^{\max}/N_{\text{cac/pack}}}{(P/M)_{\text{cac}}}$$
$$M_{\text{cac,em}} + M_{\text{cac,pe}} = P_{\text{cac}}^{\max}\left(\frac{1}{(P/M)_{\text{em}}} + \frac{1}{\eta_{\text{em}}\eta_{\text{pe}}(P/M)_{\text{pe}}}\right)$$
$$\Delta M_{e-\text{ecs}} = \kappa_{\text{ecs}} N_{\text{pack}} N_{\text{cac/pack}} (M_{\text{cac}} + M_{\text{cac,em}} + M_{\text{cac,pe}}) \tag{10}$$

where $(P/M)_{\text{cac}}$, $(P/M)_{\text{em}}$, and $(P/M)_{\text{pe}}$ are the power-to-mass ratios of these components; and η_{em} and η_{pe} are the overall efficiencies of the electric motors and power electronics. The masses of other smaller pack components that are not explicitly estimated are represented using the multiplicative factor $\kappa_{\text{ecs}} = 1.25$. For component sizing, it is assumed that each ECS pack can satisfy the requirements of the whole aircraft in case of failure of the other pack. Each ECS pack is assumed to have two compressors [42] ($N_{\text{cac/pack}} = 2$), each with a dedicated motor and power electronics. Each motor compressor is sized to be able to provide half of the pack's total mass flow capacity.

D. Electric Taxiing System

The operational requirements for sizing the ETS were set based on those identified by Airbus for the Electric Green Taxiing System (EGTS) technology demonstration program [9]. These included 1) achieving breakaway under maximum ramp weight against a specified gradient, 2) attaining a maximum taxiing speed of 20 kt, 3) accelerating from standstill to 10 kt in under 20 s, and 4) accelerating from standstill to 18 kt in 90 s. Using the preceding information, the sizing approach described by Chakraborty et al. [51] yielded the following relationships for the ETS power requirement P_{req} and mass increment Δm_{sys} as a function of the vehicle's maximum takeoff mass M_{TO}:

$$P_{\text{req}}[\text{kW}] = 4 \cdot 10^{-10} M_{\text{TO}}[\text{kg}]^2 + 0.0016 M_{\text{TO}}[\text{kg}] - 2.2971$$
$$\Delta m_{\text{sys}}[\text{kg}] = 1 \cdot 10^{-8} M_{\text{TO}}[\text{kg}]^2 + 0.0037 M_{\text{TO}}[\text{kg}] + 24.437 \tag{11}$$

The predicted power and weight showed good agreement with the published EGTS figures [9] for the Airbus A320 aircraft. The fuel saved on the ground through the use of ETS was given by

$$\Delta m_{f,\text{ets,gnd}} = -(\dot{m}_{f,\text{engs}} - \dot{m}_{f,\text{apu}}) T_{\text{ets}},$$
$$T_{\text{ets}} = T_{\text{taxi-out}} + T_{\text{taxi-in}} - T_{\text{warmup}} - T_{\text{cooldown}}, \tag{12}$$

where $\dot{m}_{f,\text{engs}}$ and $\dot{m}_{f,\text{apu}}$ are, respectively, the fuel flow rates of the main engines and the APU while taxiing; and T_{ets} is the total time for which the ETS is used. The net fuel benefit or penalty due to the incorporation of ETS is given by the relative magnitudes of $\Delta m_{f,\text{ets,gnd}}$ and the in-flight fuel penalty $\Delta m_{f,\text{ets,flt}}$ due to additional system mass.

E. Power Generation and Distribution Subsystems

The connectivity among the subsystem architecture components (shown notionally in Fig. 3a) is determined automatically by an architecture definition algorithm using heuristic rules that were identified from inspection of subsystem architectures of existing conventional aircraft and MEA. The objective of this algorithm (which is used in lieu of a formal fault tree analysis) is to rapidly determine a feasible architecture connectivity that is equivalent to that of existing aircraft from the point of view of redundancy of power consumers, power systems, and power sources. The performance of the algorithm was verified through benchmarking cases involving the subsystem architectures of some existing aircraft [52]. The connectivity among architecture elements determined by the algorithm is translated into the physical connectivity such as that shown in Fig. 6. This allows, among other things, the computation of the lengths of power distribution elements for the HPGDS, PPGDS, and EPGDS.

1. Hydraulic Power Generation and Distribution System

The progressive electrification of the actuation functions results in reduction of HPGDS mass through downsizing or elimination of hydraulic piping (power distribution elements) and hydraulic pumps (power sources). For each hydraulic connection "j" within an architecture, the connection length L_j is computed from the three-dimensional (3-D) geometric model of the aircraft, whereas the flow demand Q_j is computed based on the actuation requirements using the hydraulic power equation. Based on a study of existing Airbus aircraft, Banel-Caule [53] established that the weight of filled piping (i.e., pipes containing hydraulic fluid) is proportional to the product of flow rate and the piping length summed over all consumers. Thus, in equality form,

$$W_{\text{piping}} = \mathcal{K}_{\text{pws}} \sum_j Q_j L_j \tag{13}$$

To compute the pipe weight sensitivity factor $\mathcal{K}_{\text{pws}}$ of Eq. (13), the summation is first computed for a conventional hydraulic actuation architecture, for which an estimate of the hydraulic system weight $W_{\text{hyd}}^{\text{conv}}$ is generated by FLOPS (assuming 5000 psi system pressure). Further, from the hydraulic system weight breakdown presented by Banel-Caule [53] (Table A1), the combined weight of piping and associated couplings, brackets, manifolds, filters, and valves is seen to be a fraction ($\alpha = 0.45 + 0.24 + 0.12 = 0.81$) of the total hydraulic system weight. Thus, $W_{\text{piping}}^{\text{conv}} = \alpha W_{\text{hyd}}^{\text{conv}}$. Solving Eq. (13) for $\mathcal{K}_{\text{pws}}$ yields the pipe weight factor, which is assumed to be a constant characteristic for a given aircraft size. Using this pipe weight factor $\mathcal{K}_{\text{pws}}$, the residual piping weight $W_{\text{hyd}}^{\text{mea}}$ for MEA architectures that retain hydraulics is then computed directly using Eq. (13).

For conventional hydraulic actuation, the required pump capacity is typically determined by a sizing load case where high flow-demand loads such as landing gear, flaps, or thrust reversers must be actuated with the engines at or close to flight idle [54]. However, electrification of one or more actuation functions may affect the sizing load case, and thus the required pump capacity. To capture such dependencies, the required pump capacity is determined using a hydraulic load analysis [34] that considers both nominal and failure scenarios. This is then used to compute the weight of pumps using power-to-mass ratios identified from pump manufacturer product datasheets.

The HPGDS power dissipation, which ultimately increases the shaft-power extraction from the engines, is computed as

$$P_{\text{HPGDS}} = \left(\frac{1}{\eta_{\text{pump}}} - 1\right)\left(\sum_{i=1}^{N} P_{\text{hyd}}^{(i)} + \Delta p_{\text{nom}} Q_{\text{lkg}}\right) + \Delta p_{\text{nom}} Q_{\text{lkg}} \tag{14}$$

where η_{pump} is the pump overall efficiency. The leakage flow Q_{lkg} is modeled as a fixed fraction of the installed hydraulic capacity based on the hydraulic load profile for the Airbus A320 [55].

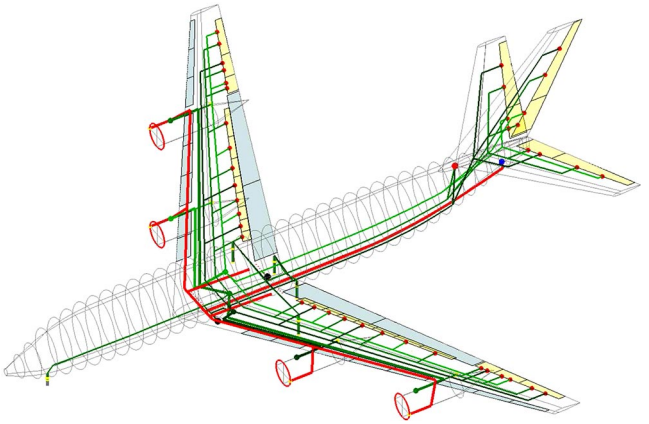

Fig. 6 Translation of architecting algorithm's connections to physical equivalents within aircraft geometric model.

2. Pneumatic Power Generation and Distribution System

Complete or partial elimination of pneumatic power requirements results in reduction in PPGDS mass through downsizing or elimination of pneumatic ducting and the precooler heat exchangers (PHXs). For a given subsystem architecture containing pneumatics, the duct lengths are computed directly from the 3-D geometric model of the aircraft. The mass flow rates through the ducts are determined based on the flow requirements of the pneumatic consumers (ECS, WIPS, or CIPS). By sizing the annular cross-section duct such that 1) its inner diameter allows the mass flow rate $\dot{m}$ to be transmitted without exceeding a maximum velocity $v_{\max}$ and 2) its wall thickness can tolerate circumferential stress corresponding to a maximum pressure $p_{\max}$, the mass of a duct of length L can be shown to be given by

$$M_{\text{duct}}(\dot{m}, L) = \kappa_{\text{inst}}\left[4\rho\left(\frac{p_{\max}}{2\sigma_{\text{eff}}}\right)\left(\frac{p_{\max}}{2\sigma_{\text{eff}}}+1\right)\left(\frac{R_a T_{\text{nom}}}{p_{\text{nom}} v_{\max}}\right)\right]\dot{m}L = \kappa_{\text{inst}}\mathcal{K}_{\text{duct}}\dot{m}L \tag{15}$$

where ρ is the duct material density, p_{nom} and T_{nom} are the nominal pressure and temperature of air through the duct, σ_{eff} is the permissible tensile strength corresponding to the operating temperature, and R_a is the gas constant for air. The installation factor κ_{inst} (here conservatively set to $\kappa_{\text{inst}} = 1.5$) accounts for 1) the weight of fittings and attachments that are not explicitly accounted for and 2) the fact that the actual ducting length is likely to be longer than the estimated length due to installation issues.

The PHX is sized by the need to remove heat from the bleed air at a maximum rate. More detailed simulations [16] established that this is a takeoff condition with failure of either an engine or a pneumatic system. Based on this, the PHX mass M_{phx} is estimated as

$$M_{\text{phx}} = \kappa_{\text{phx}}\frac{\max(\sum_i \dot{m}_{bx})}{(n_{\text{eng}}/2)}, \quad M_{\text{phx,tot}} = n_{\text{eng}} M_{\text{phx}} \tag{16}$$

in which the summation is applied to all consumers of precooled bleed air, and the denominator $n_{\text{eng}}/2$ ensures that the consumers' bleed requirements can be satisfied with only half of the total pneumatic generation capacity available subsequent to failures. The constant κ_{phx} is estimated by solving Eq. (16) for the case of a known precooler weight [56]. A summary of parameters occurring in Eqs. (15) and (16) is provided in Table A2 of the Appendix.

3. Electric Power Generation and Distribution System

For all architectures considered in this work, the EPGDS is assumed to conform to a template in which 1) generated electrical power is variable-frequency 230 VAC (volts, alternating current), 2) electrified ice protection functions (WIPS and CIPS) are supplied 230 VAC power directly, and 3) 230 VAC power is converted to ±270 VDC (volts, direct current) power using Autotransformer Rectifier Units (ATRUs) to supply electrified ECS and actuation functions. Progressive electrification of subsystems results in an expansion of the EPGDS through the addition or upsizing of 1) electrical cabling, 2) power conversion equipment, and 3) electrical generators.

The lengths of electrical cabling are computed directly from the 3-D geometric model of the aircraft, whereas the power transmitted is obtained from the requirements of the downstream power consumers. The mass of a conductor of length L transmitting peak power P_{in} is computed as

$$M_{\text{cbl}}(P_{\text{in}}, L) = \kappa_{\text{inst}}\mathcal{K}_{\text{cbl}} P_{\text{in}} L \tag{17}$$

The constant $\mathcal{K}_{\text{cbl}}$ can be shown to have units of kilograms per volt-ampere per meter. It was identified by Christou et al. [57] (who considered multiple conductors within an insulated bundle) as $1/\mathcal{K}_{\text{cbl}}^{230\,\text{VAC}} = 64.6\ \text{kVA}\cdot\text{m/kg}$ and $1/\mathcal{K}_{\text{cbl}}^{\pm 270\,\text{VDC}} = 86.8\ \text{kVA}\cdot\text{m/kg}$ for the network voltages considered. The installation factor κ_{inst} is used to account for masses of connectors and fittings (that are not computed explicitly) and for additional wiring length required to avoid obstacles.

Expansion of the EPGDS may involve the need to increase the rated capacities of the APU and main engine generators. The APU generator capacity has to be increased if the ECS is electrified or if an ETS is installed because the ground power requirements of these subsystems are provided by the APU. The required capacity of the engine-driven generators is determined through an electrical loads analysis that considers both nominal operation and one-engine-inoperative operation. Since generators can be overloaded for short durations, the sizing method assumes that the generator must be able to supply 1) electrical loads that are not short-term in nature without being overloaded and 2) short-term loads while overloaded. Once the required generator capacity is determined, the mass is computed based on the generator power-to-mass ratio, which is identified as $(P/M)_{\text{gen}} = 2.8\ \text{kVA/kg}$ [58,59]. The mass of ATRUs is estimated using the peak DC power requirements of downstream users and an ATRU power-to-mass ratio $(P/M)_{\text{atru}} = 1.54\ \text{kW/kg}$ [60].

The power dissipation occurring in the EPGDS due to component and transmission inefficiencies is computed as

$$P_{\text{EPGDS}}(t) = \left(\frac{1}{\eta_{\text{gen}}\eta_{\text{fdr}}\eta_{\text{ac}}}-1\right)\sum P_{\text{ac}}(t) + \left(\frac{1}{\eta_{\text{gen}}\eta_{\text{fdr}}\eta_{\text{atru}}\eta_{\text{dc}}}-1\right)\sum P_{\text{dc}}(t) \tag{18}$$

in which the summations are carried out over all consumers of AC and DC power. Component and transmission efficiencies occurring in this relationship are summarized in Table A3 of the Appendix.

4. Mechanical Power Generation and Distribution System

The modeling of the MPGDS is limited to the estimation of the mass and power dissipation of the accessory gearboxes. The mass is estimated using an empirical correlation developed at NASA where the gearbox mass is a function of the maximum delivered output power and the gear ratio [61]. The power dissipation is computed assuming an overall gearbox efficiency of $\eta_{\text{gb}} = 0.97$ for a modern high-performance gearbox [60].

F. Secondary Power Extraction Penalties

The extraction of secondary power from the engine (either in the form of shaft-power or bleed air) while maintaining the same thrust output results in an increase in fuel consumption (i.e., an increase in the thrust-specific fuel consumption). The magnitudes of the shaft-power and bleed air extraction penalties are dependent on the engine cycle parameters and may be evaluated using a higher-fidelity propulsion system analysis tool by factoring architecture-specific secondary power requirements into the sizing of the engine [62]. However, in this paper, to facilitate the automated investigation of a large number of subsystem architectures, the secondary power extraction penalties are estimated using a simpler approach. In this, the incremental fuel flow $\Delta\dot{w}_{f,\text{spx}}$ per engine due to total shaft-power extraction of P_{spx} is modeled based on the k_p^* approach of Scholz et al. [63] as

$$\Delta\dot{w}_{f,\text{spx}} = \dot{w}_{f,0} k_p^* \frac{P_{\text{spx}}[\text{kW}]}{N_{\text{op,eng}} T_{\text{SL}}[\text{kN}]}, \quad \text{(per engine)} \tag{19}$$

in which $\dot{w}_{f,0}$ is the basic fuel flow rate (without shaft-power extraction) for each of the $N_{\text{op,eng}}$ engines, which are assumed to contribute equally to the total shaft-power P_{spx}. The constant k_p^* was given as $k_p^* = 0.0094\ \text{N/W}$ as an average of the penalties computed at flight altitudes of 0, 10,000, 20,000, and 35,000 ft at Mach numbers of 0.30, 0.60, and 0.85 at maximum continuous thrust [63]. The incremental fuel flow $\Delta\dot{w}_{f,\text{bx}}$ due to bleed air extraction $\dot{w}_{\text{bld}} = \dot{m}_{\text{bld}} \cdot g$ per engine is computed following the method of SAE AIR 1168/8 [64] as

$$\Delta\dot{w}_{f,bx} = 0.0335\left(\frac{T_{\text{tet}}[^{\circ}R]}{2000}\frac{\dot{w}_{\text{bld}}}{N_{\text{op,eng}}}\right), \quad \text{(per engine)} \qquad (20)$$

in which T_{tet} is the turbine entry temperature, for which a representative value of 2,400° R is used in this paper. Off-take penalty relationships such as Eqs. (19) and (20) are useful because they require little additional information other than the time variation of the shaft-power and bleed air off-takes. Their limitation, however, is the fact that they are general relationships that do not account for the effect of the engine cycle parameters on the engine's sensitivity to secondary power extraction. The effect of this uncertainty on the performance of a substantially electrified subsystem architecture relative to a conventional one is assessed subsequently through a sensitivity study (Sec. V.C).

V. Assessment of Subsystem Architecture Performance

A comparative performance assessment of the subsystem architectures within the selected architecture subset (Table 2) for the three aircraft sizes considered (Table 1) is provided in Sec. V.A. Subsystem designs or solutions that appear in the best-performing subsystem architectures for each of the three aircraft sizes are presented and discussed in Sec. V.B. Finally, the sensitivity of architecture performance to the estimated penalties for secondary power extraction is assessed by comparing the performance of a substantially electrified subsystem architecture to that of a conventional one in Sec. V.C.

A. Relative Performance of Subsystem Architectures

All 512 subsystem architecture combinations present within the MOA of Table 2 are evaluated for the SSA, LTA, and VLA. In each case, the aircraft are resized to the same wing loading, thrust-to-weight ratio, and tail volume coefficients as the baseline (regardless of whether resizing improves or degrades performance). The results are summarized in Fig. 7, where the block fuel (BF), operating empty weight (OEW), and maximum ramp weight (MRW) of the architectures are shown as percentage-delta (%-Δ) quantities relative to the corresponding quantities for the baseline with conventional subsystem architecture. As a result, these conventional architectures (SSA-00000, LTA-00000, and VLA-00000) occupy the origins of the respective plots. The performance of the remaining 511 subsystem architectures relative to the conventional baseline is determined by the relative impacts of changes in systems weight, shaft-power and bleed air requirements, and direct drag penalties (through the avenues shown in Fig. 3b).

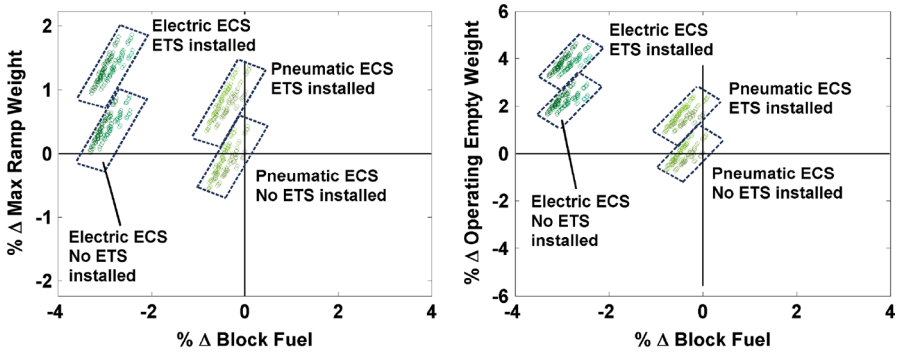

a) Relative performance of 512 subsystem architectures for SSA

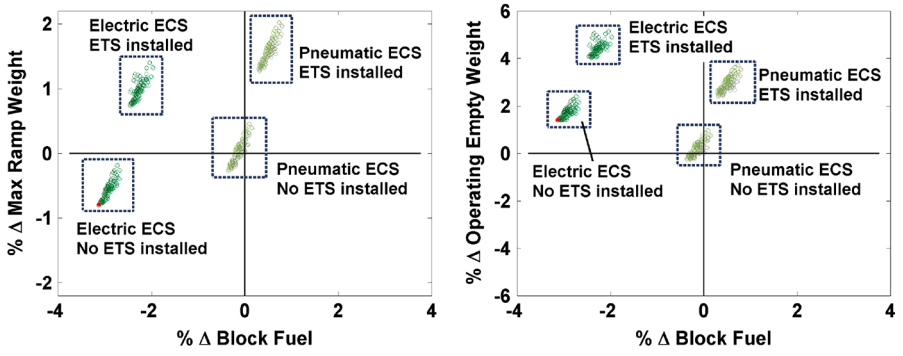

b) Relative performance of 512 subsystem architectures for LTA

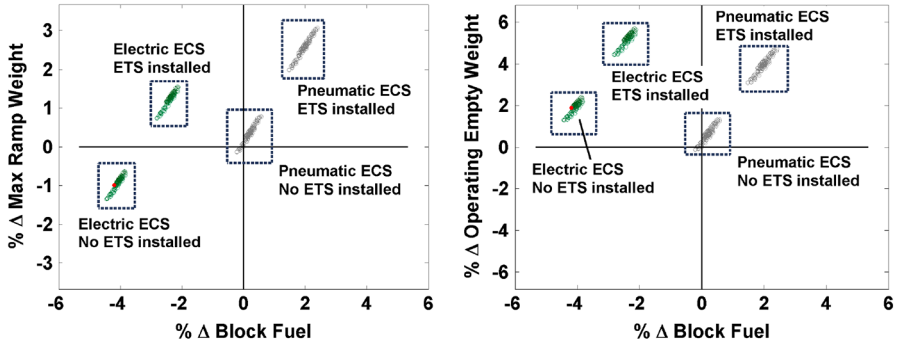

c) Relative performance of 512 subsystem architectures for VLA

Fig. 7 Comparison of 512 subsystem architectures for SSA, LTA, and VLA.

Inspection of Fig. 7 shows that, for all three vehicle sizes, the architecture combinations fall within one of four clusters. Inspection of the subsystem architectures of points within each cluster reveals that cluster affiliation is determined by the subsystem solution for the ECS (pneumatic or electric) and the presence/absence of the ETS. Each of the four clusters is described briefly:

1) Designs within cluster 1 (pneumatic ECS, no ETS installed) are in the vicinity of the origin. Some of the designs show improvements in fuel consumption relative to the baseline, whereas others show a degradation. For the SSA, the majority of the designs within this cluster show improvement in fuel consumption, whereas the reverse is true for the VLA.

2) Designs within cluster 2 (electric ECS, no ETS installed) show the greatest improvement in fuel consumption, for which the magnitude is the greatest for the VLA. For the LTA and the VLA, designs within this cluster also show reductions in MRW. For all three vehicles, architectures within this cluster have higher OEW than the baseline architecture.

3) Designs within cluster 3 (electric ECS, ETS installed) show an increase in both OEW and MRW relative to the baseline. For the SSA, this cluster is offset almost directly upward relative to cluster 2. For the LTA and VLA, however, the offset is upward and to the right. Therefore, for each LTA and VLA design within cluster 3, the fuel burn performance is worse compared to the corresponding point in cluster 2 that lacks the ETS (but has the same architecture otherwise). Essentially, this indicates that, regardless of the solutions employed for other subsystems, the inclusion of ETS for the LTA and VLA is impractical.

4) All points within cluster 4 (pneumatic ECS, ETS installed) are heavier in terms of OEW and MRW. For the LTA and VLA, designs within this cluster consume more fuel than the baseline. This indicates further that an ETS is not viable for vehicles of these sizes.

It is clear that the nature of the ECS (pneumatic or electric) and the presence/absence of the ETS determine which of the four clusters a subsystem architecture lies in. Electrification of the ECS in particular has a dominant influence on the architecture performance. This influence is not only due to the mass changes to multiple subsystems caused by ECS electrification but also due to the effect that the exchange of the bleed air requirement for the shaft-power requirement has on the thrust-specific fuel consumption (TSFC) degradation of the engine. Within a particular cluster, the variations in BF, OEW, and MRW occur due to variations in the designs of the actuation and ice protection subsystems. It is evident from Fig. 7 that the impact of these subsystems is of a smaller magnitude compared to that of the ECS. For the electrified architectures or architecture clusters that show a predicted fuel consumption improvement, it is seen that there is an increase in the OEW as well. In other words, electrification is accompanied by an increase in systems weight (and a concomitant fuel consumption penalty). However, this effect is offset by more significant fuel savings due to the TSFC improvements that occur as conventional pneumatic power users are electrified, which replaces less efficient bleed air off-take with more efficient shaft-power off-take from the engine.

B. Best-Performing Subsystem Architectures

The 10 best-performing subsystem architectures for the SSA, LTA, and VLA are listed in Table 4. For a given aircraft size, these fall within a very narrow range of fuel consumption improvement. Thus, even though the architectures are ranked in descending order of fuel consumption improvement relative to the baseline conventional architecture, the intent of this tabulation is not to determine a "winner." Instead, the intent is to permit observations regarding subsystem architecture trends, such as the following:

1) For reasons already stated previously, the electric taxiing system does not feature in any of the top architectures for the LTA and the VLA. For the SSA, however, architectures containing the ETS do make appearances. For all such architectures, a counterpart not containing the ETS is also present within the shortlist.

2) All the best-performing architectures for the SSA, LTA, and VLA contain electric environmental control systems. Referring to Fig. 7, all these architectures lie within cluster 2 for the LTA and VLA, and within either cluster 2 or cluster 3 for the SSA. The dominant effect of ECS electrification on the performance of the subsystem architecture was noted previously.

3) Regarding ice protection systems (WIPS and CIPS), the best-performing architectures avoid the use of pneumatic evaporative ice protection due to the associated bleed air penalty. There is only one exception, VLA-03010, which retains a pneumatic evaporative CIPS, which is perhaps compensated for by the presence of an electrothermal de-icing WIPS. In general, the best-performing architectures show a gravitation either toward electrothermal IPS or toward pneumatic running-wet anti-icing systems. For the SSA and LTA, in which three slats on each wing are protected, running-wet electrothermal anti-icing is avoided (due to the high electrical power requirement).

4) Regarding actuation functions, for the SSA and LTA, the presence of actuation packages 5, 6, and 7 (refer to Table 3) indicates substantial electrification of the actuation functions, including partial or complete electrification of primary control surface actuation. However, for the best-performing VLA architectures, actuation electrification never progresses beyond package 1 (electrified brakes and thrust reversers). Due to the high actuation loads for the VLA and the assumed technological SOTA (whereby electric actuators are heavier than equivalent hydraulic actuators), the mass addition to the actuation subsystems due to the fact that electrification is more significant for the VLA than for the LTA and SSA. At the same time, higher actuation loads result in higher power requirements, which increases the mass added to the electrical system (EPGDS) through electrical cabling, generator upsizing, and power conversion equipment. For the VLA, these mass additions outweigh the progressive mass deletion due to removal of the 5000 psi hydraulic system (HPGDS) beyond actuation package 1.

Despite the differences in the extent of electrification of the actuation functions between the SSA and LTA on the one hand and

Table 4 Best-performing SSA, LTA, and VLA subsystem architectures with respect to fuel consumption improvement relative to conventional subsystem architecture[a]

	SSA		LTA		VLA	
Rank	Arch.	%-Δ BF	Arch.	%-Δ BF	Arch.	%-Δ BF
1	SSA – 73310	−3.31	LTA – 73310	−3.13	VLA – 03310	−4.45
2	−73110	−3.31	−73110	−3.13	−01310	−4.43
3	−63310	−3.29	−63310	−3.11	−03110	−4.43
4	−63110	−3.29	−63110	−3.11	−01110	−4.41
5	−71310	−3.28	−71310	−3.10	−02110	−4.38
6	−73311	−3.28	−71110	−3.10	−02310	−4.36
7	−73111	−3.28	−61310	−3.08	−13310	−4.36
8	−61310	−3.26	−61110	−3.08	−11310	−4.34
9	−63311	−3.26	−53310	−3.07	−13110	−4.34
10	−63111	−3.26	−53110	−3.07	−03010	−4.33

[a]Numbering scheme is explained in Fig. 5.

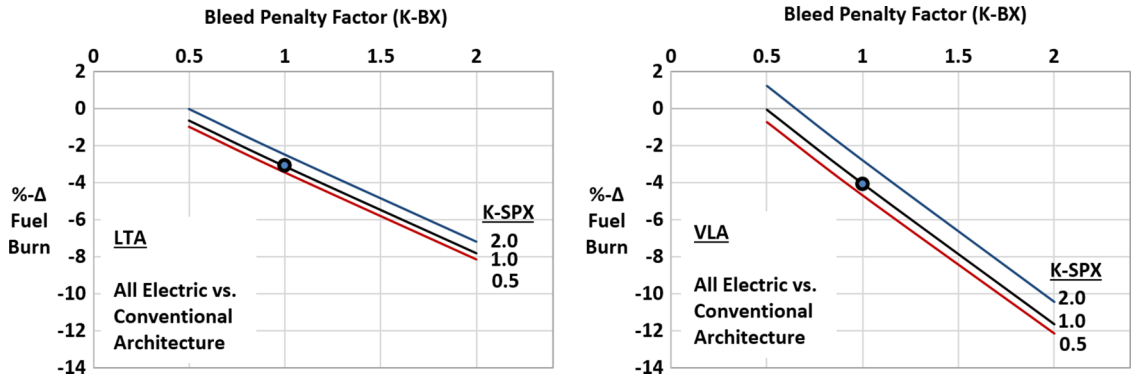

Fig. 8 Performance sensitivity of substantially electrified architecture for variation of K factors $K_{spx} \in [0,2]$ and $K_{bx} \in [0,2]$.

the VLA on the other, the following commonalities exist: the top architectures for all three aircraft sizes are either bleedless or have significantly reduced bleed requirements (through electrification of the ECS, electrification of either the WIPS or the CIPS, and the use of a running-wet design for the remaining pneumatic ice protection function).

C. Sensitivity of Architecture Performance to Secondary Power Extraction Penalties

As stated previously, the relationships of Eqs. (19) and (20) provide a first estimate of the effect of shaft-power and bleed air extraction on the fuel consumption of the engine. However, these relationships are general ones and do not, for instance, account for the effect of the engine cycle parameters on the secondary power extraction penalties. Figure 8 summarizes the results of a sensitivity study in which the impacts of variations in the off-take sensitivities on the performance of substantially electrified LTA and VLA architectures relative to conventional architectures were assessed. Thus, the following architectures are compared: 1) LTA-73310 versus LTA-00000 (Fig. 8, left) and 2) VLA-73310 versus VLA-00000 (Fig. 8, right).

To perform the sensitivity analysis, the variable $K_{spx} \in [0.5, 2]$ is introduced as a multiplicative K factor into the shaft-power extraction penalty of Eq. (19). Similarly, $K_{bx} \in [0.5, 2]$ is introduced as a multiplicative K factor into the bleed air extraction penalty of Eq. (20). Thus, the implication of $K_{spx} = 1.1$, $K_{bx} = 1.2$, for instance, is that shaft-power extraction is 10% more expensive than predicted by Eq. (19), whereas bleed air extraction is 20% more expensive than predicted by Eq. (20) (more expensive ⇒ higher fuel flow penalty).

For both the LTA and the VLA, the fuel consumption of the conventional (−00000) and electrified (−73310) subsystem architectures are evaluated for various $K_{spx} - K_{bx}$ combinations within the ranges specified previously. The block fuel %-Δ for each such combination is computed as

$$\%\text{-}\Delta\text{BF} = \frac{\text{BF}_{-73310} - \text{BF}_{-00000}}{\text{BF}_{-00000}} \tag{21}$$

The circled points in Fig. 8 indicate the relative performance of the substantially electrified and conventional LTA and VLA architectures for $K_{spx} = K_{bx} = 1.0$. It is apparent that the variation of K_{bx} has a more significant impact than that of K_{spx}, with both factors varied over the range [0.5, 2]. It is also evident that the relative performance advantage of the substantially electrified architecture (−73310) remains even when considering significant overprediction of the bleed air extraction penalty and/or significant underprediction of the shaft-power extraction penalty. For the VLA, the advantage is nullified only for a twofold overprediction of the bleed air penalty ($K_{bx} = 0.5$, $K_{spx} = 1$). For the LTA, this occurs only for a twofold overprediction of the bleed air penalty along with a twofold underprediction of the shaft-power penalty ($K_{bx} = 0.5$, $K_{spx} = 2$).

VI. Conclusions

This paper considered the simultaneous sizing and analysis of an aircraft and its subsystems in early design using the Integrated Subsystem Sizing and Architecture Assessment Capability. In particular, the ISSAAC allowed rapid assessments of the impact of novel subsystem architectures for which little or no historical data exist. This was investigated by evaluating the aircraft-level and mission-level impacts of subsystem architectures within a diverse architecture space for a small single-aisle aircraft, a large twin-aisle aircraft, and a very large aircraft.

This investigation revealed that architectures fell into distinct clusters depending on whether or not the environmental control system was electrified and whether or not an electric taxiing system was installed in the aircraft. The incorporation of the ETS within the subsystem architectures of the LTA and VLA resulted in substantial performance degradation that effectively ruled out the practicality of such a system on such larger aircraft. Electrification of the ECS had a dominant impact on subsystem architecture performance. It resulted in an increase in the operating empty weight but also a reduction in the fuel consumption primarily due to the exchange of bleed air for shaft-power. The solutions for the actuation and ice protection subsystems were seen to have impacts of a significantly lower magnitude.

For all three aircraft, the best-performing architectures were either bleedless architectures or architectures with significantly reduced bleed requirements (due to electrification of one or more pneumatic subsystems, or the use of running-wet ice protection system designs). However, the best-performing architectures for the SSA and LTA differed from those for the VLA in the extent of electrification of the actuation functions. The electrification was significant for the SSA and LTA but not for the VLA. This was due to significant mass additions to the actuation subsystems and the EPGDS due to higher actuation loads and power requirements.

A sensitivity study in which a substantially electrified architecture was compared to a conventional one revealed that the relative performance was affected by the magnitudes of the thrust-specific fuel consumption penalties associated with the extraction of shaft-power and bleed air from the engine. Although the predicted fuel burn advantage of the electrified architecture was partially nullified in the case of overprediction of the bleed air penalty and underprediction of the shaft-power penalty, significant under- and overpredictions of these penalties were required to negate the advantage completely.

One avenue for future work involves the modeling of additional subsystems along with the enhancement and refinement of the current modeling approach. The latter includes the testing of the impact of modeling assumptions, approximations, and parameter estimates on the predicted performance of subsystem architectures through sensitivity analyses. A second avenue involves a more thorough consideration of the effect of engine cycle parameters on the secondary power extraction penalties through the use of a higher-fidelity propulsion system analysis tool. A third avenue involves investigating an even larger architectural space, perhaps using a genetic algorithm to evaluate, populate, and propagate generations of high-performing architectures.

Appendix A: Schematic of ECS Pack

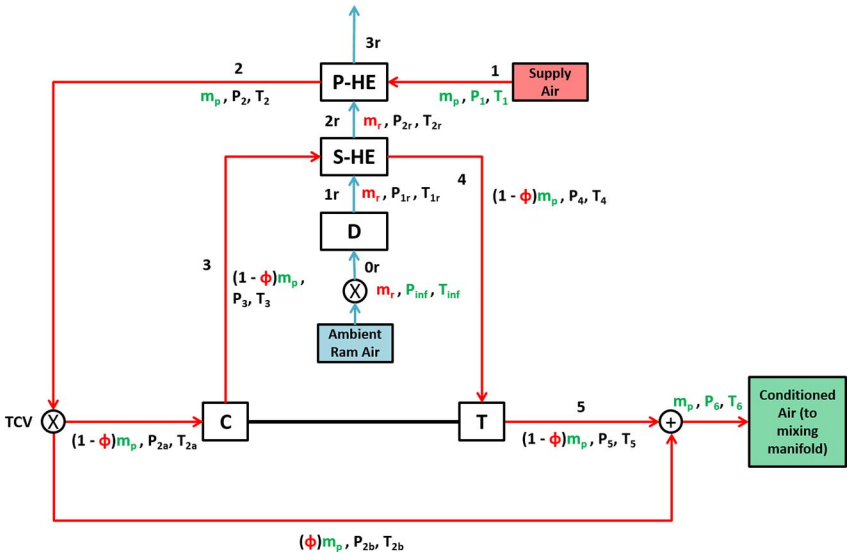

Fig. A1 ECS pack schematic (C, compressor; D, diffuser; P-HE, primary heat exchanger; S-HE, secondary heat exchanger; TCV, temperature control valve; T, turbine).

Table A1 Percentage weight breakdown of hydraulic system components [53]

Components	Weight percentage, %
Hydraulic pipes + fluid	45
Couplings + brackets	24
Manifolds + filters + valves	12
Ram air turbine	10
Miscellaneous equipment	9

Table A2 Parameter summary for PPGDS ducts [Eq. (15)] and precoolers [Eq. (16)]

Parameter	Value	Source and comments
p_{nom}	330 kPa	Refs. [62,65]
$p_{\max}$	$3.0P_{\text{nom}}$	Title 14 of CFR section 25.1438 [28]
T_{nom}	200°C	Ref. [65]
$v_{\max}$	30 m/s	Ref. [67]
ρ_{duct}	4,510 kg/m^3	Titanium Grade 2 (Ti Gr.2)/Grade 3 (Gr.3) [68]
σ_t	49.5 MPa	Mean for Ti Gr.2 and Gr.3 at T_{nom} [68]
σ_{eff}	$\sigma_t - p_{\max}(1 - Y)$	$Y = 0.4$ for nonferrous metals [68]
κ_{phx}	17.33 kg/(kg/s)	Ref. [56]

Table A3 Summary of EPGDS component efficiencies [Eq. (18)]

Component	Efficiency	Symbol	Source and comments
Variable frequency (VF) generator	0.92	η_{gen}	Ref. [60]
Power feeders	0.98	η_{fdr}	Based on [69]
ATRU	0.97	η_{atru}	Ref. [60]
AC distribution	0.95	η_{ac}	Based on [69]
DC distribution	0.98	η_{dc}	Based on [69]

References

[1] Faleiro, L., "Beyond the More Electric Aircraft," *AIAA Aerospace America*, AIAA, Reston, VA, Sept. 2005, pp. 35–40.

[2] Jones, R., "The More Electric Aircraft—Assessing the Benefits," *Journal of Aerospace Engineering*, Vol. 216, No. 5, 2002, pp. 259–269. doi:10.1243/095441002321028775

[3] Wheeler, P. W., Clare, J. C., Trentin, A., and Bozhko, S., "An Overview of the More Electrical Aircraft," *Journal of Aerospace Engineering*, Vol. 227, No. 4, 2013, pp. 578–585. doi:10.1177/0954410012468538

[4] Cronin, M., "The All-Electric Aircraft," *IEE Review*, Vol. 36, No. 8, Sept. 1990, pp. 309–311. doi:10.1049/ir:19900132

[5] Jomier, T., "More Open Electric Technologies (MOET)," Airbus Operations S.A.S. and MOET Consortium Partners Rept. FP6-030861, 2009.

[6] Cronin, M., Hays, A., Green, F., Radovcich, N., Helsley, C., and Rutchik, W., "Integrated Digital/Electric Aircraft Concepts Study," NASA CR 3841, 1985.

[7] Tagge, G., Irish, L., and Bailey, A. R., "Systems Study for an Integrated Digital/Electric Aircraft (IDEA)," NASA CR 3840, Jan. 1985.

[8] Bennett, J., Mecrow, B., Jack, A., Atkinson, D., Sheldon, S., Cooper, B., Mason, G., Sewell, C., and Cudley, D., "A Prototype Electrical Actuator for Aircraft Flaps and Slats," *2005 IEEE International Conference on Electric Machines and Drives*, IEEE Publ., Piscataway, NJ, 2005, pp. 41–47.

[9] Nicolas, Y., "eTaxi—Taxiing Aircraft with Engines Stopped," Flight Airworthiness Support Technology (FAST), Vol. 51, Jan. 2013, pp. 2–10, http://data.biitbook.com/FAST51.pdf [accessed 22 Oct. 2016].

[10] Sinnett, M., "787 No-Bleed Systems: Saving Fuel and Enhancing Operational Efficiencies," Aero, QTR_04, No. 28, 2007, pp. 6–11, http://www.boeing.com/commercial/aeromagazine/articles/qtr_4_07/AERO_Q407_article2.pdf [accessed 22 Oct. 2016].

[11] Van den Bossche, D., "The A380 Flight Control Electrohydrostatic Actuators, Achievements and Lessons Learnt," *25th International Congress of the Aeronautical Sciences*, ICAS Paper 2006-7.4.1, Hamburg, Germany, Sept. 2006.

[12] Raymer, D., *Aircraft Design: A Conceptual Approach*, 4th ed., AIAA Education Series, AIAA, Reston, VA, 2006.

[13] Roskam, J., *Airplane Design, Part V: Component Weight Estimation*, Design Analysis and Research Corp., 1999.

[14] Torenbeek, E., *Synthesis of Subsonic Airplane Design: An Introduction to the Preliminary Design of Subsonic General Aviation*

and Transport Aircraft, with Emphasis on Layout, Aerodynamic Design, Propulsion and Performance, Delft Univ. Press, Delft, The Netherlands, 1976.

[15] Lammering, T., "Integration of Aircraft Systems into Conceptual Design Synthesis," Ph.D. Thesis, Inst. of Aeronautics and Astronautics (ILR), RWTH Aachen Univ., Aachen, Germany, 2014.

[16] Liscouet-Hanke, S., "A Model-Based Methodology for Integrated Preliminary Sizing and Analysis of Aircraft Power System Architectures," Ph.D. Thesis, Univ. de Toulouse, Toulouse, France, 2008.

[17] McCullers, L., *Flight Optimization System, Release 8.11, User's Guide*, NASA Langley Research Center, Hampton, VA, Oct. 2009.

[18] Lytle, J. K., "The Numerical Propulsion System Simulation: An Overview," NASA TM-2000-209915, June 2000, http://ntrs.nasa.gov/archive/nasa/casi.ntrs.nasa.gov/20000063377.pdf [retrieved 2016].

[19] Chakraborty, I., "Subsystem Architecture Sizing and Analysis for Aircraft Conceptual Design," Ph.D. Thesis, Daniel F. Guggenheim School of Aerospace Engineering, Georgia Inst. of Technology, Atlanta, GA, Dec. 2015. https://smartech.gatech.edu/handle/1853/54427 [retrieved 2016].

[20] Chakraborty, I., and Mavris, D., "Assessing Impact of Epistemic and Technological Uncertainty on Aircraft Subsystem Architectures," *AIAA Aviation 2016 Conference*, AIAA Paper 2016-3145, June 2016.

[21] Chakraborty, I., and Mavris, D., "Integrated Assessment of Aircraft and Novel Subsystem Architectures in Early Design," *AIAA Science and Technology Exposition and Forum (SciTech)*, AIAA Paper 2016-0215, Jan. 2016.

[22] Chakraborty, I., Mavris, D., Emeneth, M., and Schneegans, A., "An Integrated Approach to Vehicle and Subsystem Sizing and Analysis for Novel Subsystem Architectures," *Journal of Aerospace Engineering*, Vol. 230, No. 3, 2016, pp. 496–514.

[23] Rudolph, P., "High Lift Systems on Subsonic Commercial Airliners," NASA CR 4746, Sept. 1996.

[24] Roskam, J., *Airplane Design, Part VI: Preliminary Calculation of Aerodynamic, Thrust and Power Characteristics*, Design Analysis and Research, 1999.

[25] Scholz, D., "Development of a CAE-Tool for the Design of Flight Control and Hydraulic Systems," *AeroTech '95*, Inst. of Mechanical Engineers Paper C505/9/011, London, Oct. 1995.

[26] Simsic, C., "Electric Actuation System Duty Cycles," *Proceedings of the IEEE 1991 National Aerospace and Electronics Conference, 1991 (NAECON 1991)*, Vol. 2, IEEE Publ., Piscataway, NJ, 1991, pp. 540–545.

[27] Collins, A., "EABSYS: Electrically Actuated Braking System," *IEE Colloquium on Electrical Machines and Systems for the More Electric Aircraft*, The Inst. of Engineering and Technology (IET), London, 1999, p. 4.

[28] "Aeronautics and Space," Airworthiness Standards: Transport Category Airplanes, Pt. 25, Title 14, Code of Federal Regulations, Federal Aviation Administration, U.S. Dept. of Transportation, Oct. 2016.

[29] *Aircraft Tire Data Book*, Goodyear Tire, and Rubber Co., Akron, OH, 2002.

[30] Currey, N., *Aircraft Landing Gear Design: Principles and Practices*, AIAA Education Series, AIAA, New York, 1988.

[31] Cameron-Johnson, A., "Some Aspects of the Design of Aircraft Steering Systems," *Aircraft Engineering and Aerospace Technology*, Vol. 43, No. 6, 1971, pp. 7–10. doi:10.1108/eb034778

[32] Jenkins, S., "Landing Gear Design and Development," *Journal of Aerospace Engineering*, Vol. 203, No. 1, 1989, pp. 67–73.

[33] Li, W., and Fielding, J., "Preliminary Study of EMA Landing Gear Actuation," *28th Congress of the International Council of the Aeronautical Sciences*, ICAS Paper 2012-6.8.2, Brisbane, Australia, 2012.

[34] Scholz, D., "MPC 75 Hydraulic Load Analysis," Deutsche Airbus TN-EV52-362/91, Hamburg, Germany, July 1991.

[35] Socheleau, J., Mare, J.-C., and Baudu, P., "Actuation Technologies and Application—Flight Controls and Thrust Reverser Actuation," *Technologies for Energy Optimized Aircraft Equipment Systems (TEOS Forum)*, Power Optimized Aircraft (POA) Project Consortium, Session 6A, Paris, 2006.

[36] Al-Khalil, K., Horvath, C., Miller, D., and Wright, W., "Validation of Thermal Ice Protection Computer Codes: Part 3—The Validation of ANTICE," *35th Aerospace Sciences Meeting and Exhibit*, AIAA Paper 1997-0051, 1997.

[37] Krammer, P., and Scholz, D., "Estimation of Electrical Power Required for Deicing Systems," Hamburg Univ. of Applied Sciences (HAW) Aero_TN_Deicing_09-07-14, Berliner, Hamburg, 2009.

[38] "Certification Specifications and Acceptable Means of Compliance for Large Aeroplanes: CS-25, Amendment 16," European Aviation Safety Agency, 2013, Appendix C.

[39] Jeck, R., "Icing Design Envelopes (14 CFR Parts 25 and 29, Appendix C) Converted to a Distance-Based Format," Federal Aviation Administration, Airport and Aircraft Safety Research and Development, William J. Hughes Technical Center Final Rept. DOT/FAA/AR-00/30, 2002.

[40] Gray, V., "Correlations Among Ice Measurements, Impingement Rates, Icing Conditions, and Drag Coefficients for Unswept NACA 65A004 Airfoil," NACA TN 4151, Washington, D.C., Feb. 1958.

[41] Colin, A., Herzog, J., Dodds, G., and Larue, F., "Environmental Control System and Wing Ice Protection (ECS and WIPS)," *Technologies for Energy Optimized Aircraft Equipment Systems (TEOS Forum)*, Power Optimized Aircraft (POA) Project Consortium, Session 5A, Paris, 2006.

[42] Nelson, T., "787 Systems and Performance," *Flight Operations Engineering*, Boeing Commercial Airplanes, Seattle, WA, March 2009, http://myhres.com/Boeing-787-Systems-and-Performance.pdf [retrieved 4 Nov. 2015].

[43] Hunt, E., Reid, D., Space, D., and Tilton, F., "Commercial Airliner Environmental Control System—Engineering Aspects of Air Quality," *Annual Meeting of the Aerospace Medical Association*, Anaheim, CA, 1995.

[44] Muller, C., Scholz, D., and Giese, T., "Dynamic Simulation of Innovative Aircraft Air Conditioning," *First CEAS European Air and Space Conference*, Council of the European Aerospace Societies (CEAS), Berlin, Sept. 2007.

[45] Pratt, J., Klebanoff, L., Munoz-Ramos, K., Akhil, A., Curgus, D., and Schenkman, B., "Proton Exchange Membrane Fuel Cells for Electrical Power Generation On-Board Commercial Airplanes," Sandia National Labs. Rept. SAND2011-3119, Albuquerque, NM, May 2011.

[46] "Air Conditioning, Pressurization, and Ventilation," Airbus A320 Simulator Flight Crew Operating Manual, Airbus Industries, http://www.smartcockpit.com/aircraft-ressources/A320-Air_Conditioning_and_Pressurization.html [retrieved 4 Nov. 2015].

[47] "Air Conditioning, Pressurization, and Ventilation," Airbus A330 Simulator Flight Crew Operating Manual, Airbus Industries, http://www.smartcockpit.com/aircraft-ressources/A330-Aircond-Press-Vent.html [retrieved 4 Nov. 2015].

[48] "Air Conditioning, Pressurization, and Ventilation," Airbus A340 Simulator Flight Crew Operating Manual, Airbus Industrie, http://www.smartcockpit.com/aircraft-ressources/FCOM_A340-Air_Cond-Press-Vent.html [retrieved 4 Nov. 2015].

[49] "Boeing 737 NG—Systems Summary [Air Systems]," The Boeing Company, http://www.smartcockpit.com/aircraft-ressources/B_NG-Air_Systems.html [retrieved 4 Nov. 2015].

[50] Brasseur, A., Leppert, W., and Pradille, A., "Inside the 747-8 New Environmental Control System," Aero, QTR_1, No. 45, 2012, pp. 18–25, http://www.boeing.com/commercial/aeromagazine/articles/2012_q1/pdfs/AERO_2012q1_article4.pdf [retrieved 2016].

[51] Chakraborty, I., LeVine, M., and Hassan, M., "Assessing Taxiing Trade Spaces from Aircraft, Airport, and Airline Perspectives," *AIAA Aviation 2015 Conference*, AIAA Paper 2015-2386, June 2015.

[52] Chakraborty, I., and Mavris, D., "Heuristic Definition, Evaluation, and Impact Decomposition of Aircraft Subsystem Architectures," *AIAA Aviation 2016 Conference*, AIAA Paper 2016-3144, June 2016.

[53] Banel-Caule, I., "Systems Weight Estimation Enhanced Method for Early Project Phases," *66th Annual Conference of Society of Allied Weight Engineers, Inc.*, Society of Allied Weight Engineers Paper 3430, Madrid, May 2007.

[54] Biedermann, O., and Geerling, G., "Power Control Units with Secondary Control Hydraulic Motor—A New Concept for Application in Aircraft High Lift Systems," *Proceedings of the Conference on Recent Advances in Aerospace Hydraulics*, Toulouse, France, 1998, pp. 73–78, http://citeseerx.ist.psu.edu/viewdoc/download?doi=10.1.1.544.3909&rep=rep1&type=pdf [accessed 22 Oct. 2016].

[55] Airbus A320 Aircraft Maintenance Manual, ATA29, Airbus Industries, 2006.

[56] "Boeing 777 Aircraft Maintenance Manual," *Pneumatic*, Boeing Commercial Airplanes, Seattle, WA, 2006, Chap. 36.

[57] Christou, I., Nelms, A., Cotton, I., and Husband, M., "Choice of Optimal Voltage for More Electric Aircraft Wiring Systems," *IET Electrical Systems in Transportation*, Vol. 1, No. 1, 2011, pp. 24–30. doi:10.1049/iet-est.2010.0021

[58] Xia, X., "Dynamic Power Distribution Management for all Electric Aircraft," M.S. Thesis, School of Engineering, Cranfield Univ., Cranfield, England, U.K., 2011.

[59] Martinez, M., Sawata, T., Rouge-Carrassat, T., and Blineau, J.-M., "Electrical Power Sources and Aircraft Power Networks," *Technologies*

for Energy Optimized Aircraft Equipment Systems (TEOS Forum), Power Optimized Aircraft (POA) Project Consortium, Session 2C, Paris, 2006.

[60] Whyatt, G., and Chick, L., "Electrical Generation for More-Electric Aircraft Using Solid Oxide Fuel Cells," Pacific Northwest National Lab. Rept. PNNL-21382, Richland, WA, April 2012.

[61] Hendricks, E., and Tong, M., "Performance and Weight Estimates for an Advanced Open Rotor Engine," NASA TM-2012-217710, NASA John H. Glenn Research Center, Cleveland, OH, Sept. 2012.

[62] Ozcan, M., Chakraborty, I., and Mavris, D., "Impact of Subsystem Secondary Power Requirements on Gas Turbine Sizing and Performance," *AIAA Aviation 2016 Conference*, AIAA Paper 2016-3146, June 2016.

[63] Scholz, D., Seresinhe, R., Staack, I., and Lawson, C., "Fuel Consumption due to Shaft Power Off-Takes from the Engine," *4th International Workshop on Aircraft System Technologies, AST 2013*, Shaker Verlag GmbH, Kaiserstraße, Herzogenrath, Germany, April 2013, pp. 169–179.

[64] "SAE Aerospace Applied Thermodynamics Manual—SAE AIR 1168," Society of Automotive Engineers, Warrendale, PA, 1989.

[65] "Pneumatic," Airbus A330 Flight Crew Operating Manual," Airbus Industries, http://www.smartcockpit.com/aircraft-ressources/A330-Pneumatic.html [retrieved 4 Nov. 2015].

[66] "Airbus A319/A320/A321: Pneumatics," http://www.smartcockpit.com/aircraft-ressources/A319-320-321-Pneumatics.html [retrieved 4 Nov. 2015].

[67] Ramgopal, M., "Design of Air Conditioning Ducts," Refrigeration and Air Conditioning, Lesson 38, Indian Inst. of Technology, Kharagpur, India, http://nptel.ac.in/courses/112105129/pdf/RandAC%20Lecture%2038.pdf [retrieved 4 Nov. 2015].

[68] Peacock, D., "Effective Design Using Titanium," *International Conference on Titanium in Practical Applications*, Norwegian Association of Corrosion Engineers, 1990.

[69] "Acceptable Methods, Techniques, and Practices—Aircraft Inspection and Repair," U.S. Dept. of Transporation, Federal Aviation Administration, Advisory Circular 43.13-1B, Sept. 1998.